Standing Wave Analysis of SMB Chromatography: Linear Systems

Z. Ma and N.-H. L. Wang
School of Chemical Engineering, Purdue University, West Lafayette, IN 47907

The concept of standing concentration waves is introduced to derive design equations for continuous moving bed (CMB) processes. For linear isotherm systems, simple equations are derived from the analysis to link product purity and recovery to zone lengths, bed movement velocity, flow rates, column capacity factors, and mass-transfer coefficients. Once product purity, recovery and feed flow rate are specified for a given system, the zone flow rates and bed movement velocity that provide the highest throughput and the lowest solvent consumption can be determined from the solutions. In a given system, there is a trade-off between product purity and throughput. If bed volume and product purities are fixed, the longer the zone lengths, the higher the throughput. Simulations based on a linear driving force model that considers axial dispersion and lumped film and intraparticle diffusion are used to compare the column profiles and effluent histories of CMB and simulated moving bed (SMB). A numerical algorithm is introduced to allow simulation of both CMB and SMB operations using the same program. The comparison shows that the design equations derived for CMB systems are applicable to SMB systems. Finally, the standing wave solutions are used to analyze an experimental SMB system from the literature (Ching et al., 1991). Simulations agree closely with the data and the predictions of the theoretical analysis.

Introduction

Since the successful commercialization of the UOP Molex and Parex processes for hydrocarbon purification (Broughton, 1968; Broughton et al., 1970), the number of applications of simulated moving-bed (SMB) chromatography has been growing steadily (Ganetsos and Barker, 1993). The use of SMB for the separation of fructose from dextrose (Corbett and Burke, 1996), resolution of enantiomers (Ching et al., 1993), protein desalting (Hashimoto et al., 1988), production of high-fructose syrup (Hashimoto et al., 1983), multicomponent separation of sucrose, glucose, and fructose (Kishihara et al., 1992), and many others have been reported in the literature (Adachi, 1994; Ruthven and Ching, 1989).

In these applications, the system configurations can be represented by the four-zone system shown in Figure 1a (Ruthven and Ching, 1989). In such a system, the inlet and outlet ports are periodically moved along the solvent flow direction at a time-averaged linear velocity less than that of the solvent. As in fixed-bed chromatography, separation occurs because a low-affinity solute (solute 1) migrates along the direction of solvent flow faster than a high-affinity solute (solute 2) (Wankat, 1994). If the averaged feed port movement is faster than that of the high-affinity solute and slower than that of the low-affinity solute, the high-affinity solute moves backward, while the low-affinity solute moves forward with respect to the feed port. If the movement of the ports is synchronized, solute migration in a SMB is similar to that in a countercurrent operation, but without any physical movement of the sorbent. SMB has the advantages of both the fixed-bed and the moving-bed operations. It eliminates the difficulty in moving the solid phase, and is flexible in the assembly of different configurations according to specific applications while providing continuous operation (Ruthven and Ching, 1989). SMB is capable of providing high-purity products, because mixed bands are circulated in the system (zones IV to I, in Figure 1b) and only completely resolved portions of the two bands (zones II and III) are drawn out from the product ports. Sorbent utilization, solvent consumption, and mass-transfer rates can be maximized by appropriate designs

Correspondence concerning this article should be addressed to N.-H. L. Wang.

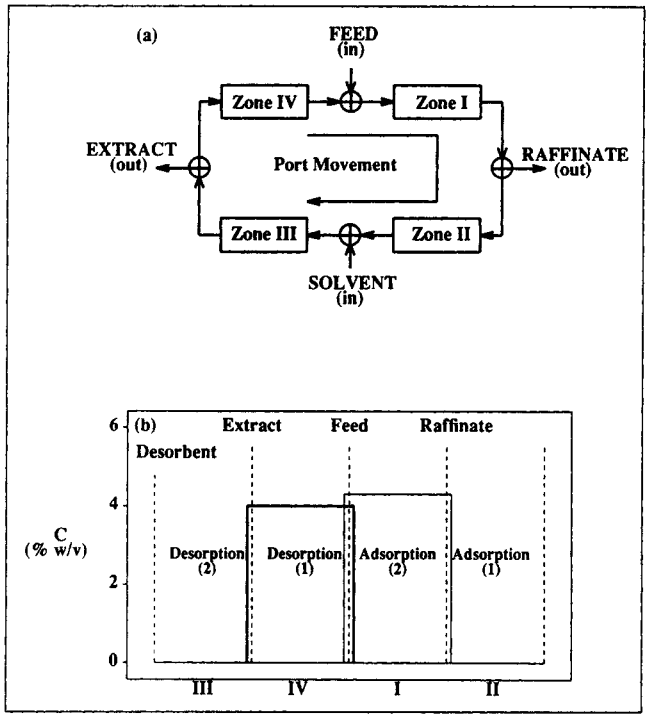

Figure 1. (a) Four-zone SMB system; (b) standing waves (thin lines, solute 1; thick lines, solute 2).

of zone lengths, flow rates, and port switching time. For these reasons, SMB is much more efficient than conventional batch chromatography (Ruthven and Ching, 1989; Ganetsos and Barker, 1993).

Although many applications of SMB chromatography have been reported (Adachi, 1994; Ruthven and Ching, 1989), an optimal design for a given separation remains difficult. Particularly, it is difficult to find the optimal flow rates and port switching time when mass-transfer resistances are dominant. The main reason is that there are many system and operating parameters to be determined, and SMB performance is highly sensitive to system configuration, operational parameters, and the mass-transfer parameters. Computer simulation and mathematical modeling have been proposed in the literature to improve fundamental understanding of SMB systems. The following two approaches are usually used: (1) continuous moving bed (CMB) analysis (Rhee et al., 1971; Ruthven, 1983; Ching and Ruthven, 1985; Hotier, 1996; Storti et al., 1993), which assumes that the solid phase moves countercurrently with respect to the desorbent flow; and (2) periodic moving port analysis, which assumes that individual fixed beds are connected with two input and two output ports with periodic port movement along the flow direction (Hashimoto et al., 1988; Charton et al., 1995; Chu and Hashim, 1995; Storti et al., 1989). The former approach is advantageous because: (1) analytical solutions can be derived and can provide significant fundamental understanding of the CMB operations; (2) the simulation algorithm is simple and easy to implement. However, this approach can only give smooth concentration effluent histories, which are far from the cyclic concentration effluent histories in SMB systems (Chu and Hashim, 1995). In the periodic moving-port approach, it is impossible to obtain closed-form analytical solutions, and numerical simulations have to be used. However, it can be employed to simulate both CMB and SMB. Obviously, the periodic moving-port approach is more realistic for SMB systems than the CMB approach.

In either approach, both the lumped mass-transfer-rate models (Ching and Ruthven, 1985; Ching et al., 1985; Storti et al., 1995) and the staged models (Ulrich and Hsu, 1989; Charton et al., 1995) have been used. Nevertheless, in all the approaches, the flow rates and port-switching time have to be derived from the equilibrium theory (which neglects the effects of axial dispersion and other mass-transfer resistances). Since equilibrium theory cannot link product purities to zone flow rates, zone lengths, and mass-transfer parameters, the resulting design can only serve as an initial guess for further refinement with iterative numerical simulations (Storti et al., 1995). The McCabe-Thiele diagram (Ruthven and Ching, 1989) can be used to search for the conditions that guarantee complete separation. However, such an approach is also based on the assumption of equilibrium operations. Although zone lengths can be determined from the height of an equivalent theoretical plate (HETP) (Ruthven and Ching, 1989), product purities cannot be determined *a priori* and have to be found by repeated iteration. In both approaches, the search of the zone flow rates, switching time, and the zone lengths that guarantee the desired product purities requires trial and error. For systems with large separation factors, it is relatively easy to search for the conditions that give desired product purities, because separations are easy to achieve. For systems that have small separation factors and require high product purities as in pharmaceutical and biotechnology applications (Adachi, 1994), the literature methods are time-consuming.

Ruthven (1983) has provided a steady-state solution to a lumped linear-driving-force model for CMB systems with linear isotherms. The solution can be used to calculate product purities. However, the solution is limited to systems with large Peclet and Stanton numbers. Instead of steady-state concentrations at the feed position, bulk feed concentrations are used in the solution and the steady-state concentrations at the feed position can only approach the bulk feed concentrations at very large Peclet and Stanton numbers under the conditions for complete separations (Ruthven and Ching, 1989). Kubota et al. (1989) modified the solution from Ruthven and included the unknown steady-state concentrations at the feed position with mass balances between the input and the output ports, but a numerical procedure has to be employed to find the solutions. Recently, Zhong and Guiochon (1996) have discussed analytical solutions for SMB systems based on an ideal model that neglects axial dispersion and any other mass-transfer resistances. So far, solutions that explicitly relate product purity and recovery to flow rates, moving-bed velocities, zone lengths, column-capacity factors, and mass-transfer parameters have not been reported.

In this study, a standing concentration wave concept is introduced to derive the analytical solutions at steady state for linear CMB systems. Explicit algebraic equations are derived to link product purity and recovery to (1) axial dispersion and other mass-transfer coefficients, (2) the four zone lengths, (3) the linear velocities in the four zones, and (4) the bed movement velocity. These velocities give the highest throughput

and the lowest solvent consumption when product purity and feed flow rate are specified for a given system. This approach significantly shortens the search of an optimal design in a space with ten design and operating parameters. This method is also robust, simple, and easy to implement. In contrast, the methods in the literature use an iterative search that would require numerical simulations (Storti et al., 1995; Ruthven and Ching, 1989), which are time-consuming for the development of SMB technology for new applications. A numerical algorithm is presented using the periodic moving-port approach for the simulation of both SMB and CMB systems. Numerical simulations are performed (1) to validate the analytical solutions at steady state for CMB systems; and (2) to compare the performance of SMB designs based on the analytical solutions for CMB to ensure that the standing wave design criteria for CMB systems apply to SMB systems. Finally, the newly derived criteria are utilized to analyze an experimental system from the literature (Ching et al., 1991).

Theory

In this section, the standing wave concept is first introduced and followed by obtaining the steady-state solutions for the following two types of CMB systems: (1) equilibrium systems, in which axial dispersion and other mass-transfer effects are negligible; and (2) nonequilibrium systems, in which both axial and mass transfer resistances are dominant.

Equations for continuous moving bed (CMB) systems

Mass Balance for the Mobile Phase within a Zone. In CMB, the sorbent phase moves countercurrently with respect to the mobile phase. The transport equation for a solute in the mobile phase in zone I can be derived for a stationary coordinate system, as,

$$\frac{\partial c_{bi}}{\partial t} = E_{bi}^{\mathrm{I}} \frac{\partial^2 c_{bi}}{\partial x^2} - \bar{u}_0^{\mathrm{I}} \frac{\partial c_{bi}}{\partial x} - PK_{fi}^{\mathrm{I}}(c_{bi} - c_i^*), \qquad (1)$$

where c_{bi} and c_i^* are the mobile and average pore phase concentrations of the ith component, respectively; P is the bed phase ratio, $(1-\epsilon_b)/\epsilon_b$; ϵ_b is the interstitial void fraction; and $\bar{u}_0^{\mathrm{I}}$ is the interstitial linear mobile phase velocity along the axial direction (x). The sorbent movement velocity ν is along the $(-x)$ direction. The input and output ports remain stationary in this coordinate system. Equations for other zones are the same as Eq. 1 except that the values of E_b, K_f, and $\bar{u}_0$ are different. For a fixed-bed or SMB system discussed later, the interstitial velocity relative to the sorbent phase, u_0, is the velocity that controls the propagation of concentration waves relative to the sorbent phase. These two velocities are related by $u_0^{\mathrm{I}} = \bar{u}_0^{\mathrm{I}} + \nu$. To link CMB to SMB, $\bar{u}_0^{\mathrm{I}}$ in Eq. 1 is replaced by $u_0^{\mathrm{I}} - \nu$ in the following analysis.

Mass Balance for the Pore Phase within a Zone. The following equation for the lumped mass-transfer model is proposed for a CMB process. Similar equations for batch processes can be found in Santacesaria et al. (1982):

$$\epsilon_p \frac{\partial c_i^*}{\partial t} + (1-\epsilon_p)\frac{\partial q_i^*}{\partial t} = K_{fi}^{\mathrm{I}}(c_{bi} - c_i^*) + \nu\epsilon_p \frac{\partial c_i^*}{\partial x} + (1-\epsilon_p)\nu \frac{\partial q_i^*}{\partial x}, \qquad (2)$$

where ϵ_p is the intraparticle void fraction. Equations 1 and 2 give the set of equations for CMB processes with lumped mass-transfer resistance. Note that for linear systems at local equilibrium, $q_i^* = K_i c_i^*$, where K_i is the linear equilibrium constant.

Mass Balance Equations for Systems without Mass-transfer Resistances. When axial dispersion and mass-transfer resistance are negligible, the following equation for systems with linear isotherms can be derived from Eqs. 1 and 2:

$$(1+P\delta_i)\frac{\partial c_{bi}}{\partial t} + [u_0^{\mathrm{I}} - \nu(1+P\delta_i)]\frac{\partial c_{bi}}{\partial x} = 0, \qquad (3a)$$

where

$$\delta_i \equiv \epsilon_p + (1-\epsilon_p)K_i. \qquad (3b)$$

The linear velocity of a concentration wave relative to the feed port is,

$$u_{wi} \equiv u_{si} - \nu, \qquad (4)$$

where

$$u_{si} = \frac{u_0}{1+P\delta_i}. \qquad (5)$$

Note that u_w can be positive, negative, or zero depending on the relative movement of the sorbent and the solvent. Careful examination of Eq. 4 reveals the following: (1) a concentration wave can be a standing wave with respect to the feed port if the flow rate satisfies the condition, $u_{wi} = 0$; furthermore, (2) the equation implies that in a linear system N species can be made stationary if N zones with N different flow rates are used; and (3) u_{wi} is determined by two *independent* linear velocities: the solid movement velocity, ν, and the solute movement velocity, u_{si}, which can be determined from an independent batch elution experiment (deRosset et al., 1976).

The standing wave concept is general and an analysis based on this concept can be extended to systems with nonlinear isotherms (Ma et al., 1997) and other configurations. This study is focused on binary systems with linear isotherms and the four-zone configuration, as shown in Figure 1a.

Design constraints on zone flows

Flow-rate Balance In Between Zones. In order to have continuous feed into a system in Figure 1a, the flow rates in the four zones have to satisfy the following conditions:

$$F^{\mathrm{I}} > F^{\mathrm{II}} \qquad (6)$$

$$F^{\mathrm{II}} < F^{\mathrm{III}} \qquad (7)$$

$$F^{III} > F^{IV} \tag{8}$$

$$F^{IV} < F^{I}. \tag{9}$$

Furthermore, in order to have separation, in addition to Eqs. 6 to 9, the migration velocities of the two solutes have to be taken into account in determining the zone flow rates. The following conditions for the velocities in each zone are known from the literature (Wankat, 1994).

$$u_{s2}^{I} - \nu < 0 \tag{10}$$

$$u_{s1}^{II} - \nu < 0 \tag{11}$$

$$u_{s2}^{III} - \nu > 0 \tag{12}$$

$$u_{s1}^{IV} - \nu > 0, \tag{13}$$

where u_{s2}^{I} and u_{s2}^{III} are the linear velocities of component 2 in zones I and III, respectively. The same convention is used for component 1 in zones II and IV. Equations 10 and 11 indicate that the migration velocity wave of the more retained solute (component 2) should be less than ν is zone I and that of the less retained solute (component 1) should be less than ν in zone II. Equations 12 and 13 indicate that the velocity of solute 2 should be greater than ν in zone III and that of solute 1 in zone IV. Equations 10 to 13 define all the feasible linear velocities and the bed velocities needed to guarantee separation. *Note that Eqs. 10 to 13 must be satisfied in order to have separation for systems with or without mass-transfer resistances.*

Linear velocities achieving standing waves

Equilibrium Systems without Axial Dispersion and Mass-transfer Resistances.. Equations 10 to 13 define an infinite number of solute migration velocities and bed velocities that guarantee separation. In practice, however, a specific set of linear velocities is required. Note that if the adsorption wave of solute 2 is standing still in zone I (see Figure 1b), that is, $u_{s2}^{I} = \nu$, separation occurs because the adsorption wave of solute 1 travels faster than that of solute 2, passing the raffinate port and entering zone II. Similarly, if the linear velocity is chosen such that the desorption wave of solute 1 is standing still in zone IV, that is, $u_{s1}^{IV} = \nu$, the dsorption wave of solute 2 passes the extract port and enters zone III, because the migration velocity of solute 2 is slower than that of solute 1. If the linear velocities are chosen such that the adsorption wave of solute 1 stands in zone II and the desorption wave of solute 2 stands in zone III, that is, $u_{s1}^{II} = \nu$ and $u_{s2}^{III} = \nu$, the two concentration waves are confined in their respective zones, preventing them from crossing the desorbent port and causing contamination of the products (note separations occur only in zones I and IV). To achieve the four standing waves, the zone linear velocities should satisfy the following:

$$u_0^{I} = (1 + P\delta_2)\nu \tag{14}$$

$$u_0^{II} = (1 + P\delta_1)\nu \tag{15}$$

$$u_0^{III} = (1 + P\delta_2)\nu \tag{16}$$

$$u_0^{IV} = (1 + P\delta_1)\nu. \tag{17}$$

Notice that Eqs. 14 to 17 correspond to the boundary values defined in Eqs. 10 to 13. Any other values that satisfy Eqs. 10 to 13 result in lower u_0^{I} and u_0^{II} and higher u_0^{III} and u_0^{IV}, and in turn result in a lower feed flow rate and a higher solvent flow rate for a fixed ν. Therefore, Eqs. 14 to 17 define the highest feed flow rate and lowest solvent flow rate for a given system. In practice, the feed flow rate, F^{feed}, is usually given. As a result, the difference between u_0^{I} and u_0^{IV} must satisfy,

$$\frac{F^{feed}}{\epsilon_b S} = u_0^{I} - u_0^{IV}. \tag{18}$$

Notice there are now five equations (Eqs. 14 to 18) for five unknowns, u_0^{I}, u_0^{II}, u_0^{III}, u_0^{IV}, and ν. For a fixed feed flow rate, the bed movement velocity can be found as

$$\nu = \frac{F^{feed}}{SP\epsilon_b(\delta_2 - \delta_1)}, \tag{19}$$

and then the four linear velocities can be determined from Eqs. 14 to 17.

Note Eq. 19 includes column parameters (bed porosity and column cross-sectional area), switching time, and feed flow rate, which are all the crucial parameters in a practical design. Because equilibrium is assumed, the preceding equations can only be applied to cases where the band-broadening effects, which include extracolumn dispersion, intracolumn axial dispersion, and other mass-transfer resistances, are negligible. Note also that $u_0^{I} = u_0^{III}$ and $u_0^{II} = u_0^{IV}$. Therefore, Eqs. 14 to 19 give the same flow rates of feed, raffinate, extract, and solvent. Also, if axial dispersion and other mass-transfer effects are negligible, Eqs. 14 to 17 give the optimal linear velocities (largest feed and smallest desorbent flows) for a given system. In this case, pure products at both output ports can be obtained; any finite column or zone length will produce pure products because there is no dispersion and the concentration waves are square waves with infinitely sharp boundaries (Figure 1b).

Linear Velocities in Systems with Axial Dispersion and Mass-Transfer Resistances. In a binary system without any mass-transfer resistance (equilibrium systems), there are only four different wave velocities (Figure 1b) and the four waves need to be stationary for a complete separation (Eqs. 14 and 17). In contrast, in a system with significant mass-transfer resistances (nonequilibrium systems), instead of the square waves the band boundaries are spread. Equations 14 to 17 have to be modified to take into account the mass-transfer effects. Steady state solutions of Eqs. 1 and 2 can provide the concentration profiles, which in turn can be used to find the conditions that lead to the standing waves and guarantee high product purities. The steady-state analysis is advantageous because (1) analytical solutions can be obtained; (2) in a linear system, the transient concentration profiles are continuously increasing at all positions over time (see Figures 3a and 3b); the two product concentrations at the output ports increase faster than those of the minor components, which are maximum at the steady state. Therefore, the least pure products are obtained at the steady state. If a system is designed with conditions derived from the steady-state solutions, any

time before the steady state is reached, better product purities can be obtained.

In the following, the steady-state solutions are derived for the concentration waves for solute 1 in zones II and IV and for solute 2 in zones I and III. The solutions of the concentration waves in zones I and IV are considered first because (1) separations occur only in zone I and IV; and (2) solute 2 at the raffinate port and solute 1 at the extract port are the minor components or impurities.

In a linear isotherm system with finite E_b and K_f, the following steady-state equations for solute 2 in zone I can be derived from Eqs. 1 and 2 (see the Appendix):

$$[u_0^{\mathrm{I}} - (1+P\delta_2)\nu]\frac{dc_{b2}}{dx} = \left(E_{b2}^{\mathrm{I}} + \frac{P\nu^2\delta_2^2}{K_{f2}^{\mathrm{I}}}\right)\frac{d^2c_{b2}}{dx^2}, \quad (20a)$$

$$c_{b2}(\infty) = 0, \qquad c_{b2}(0) = c_{s2}, \quad (20b)$$

and similarly for solute 1 in zone IV:

$$[u_0^{\mathrm{IV}} - (1+P\delta_1)\nu]\frac{dc_{b1}}{dx} = \left(E_{b1}^{\mathrm{IV}} + \frac{P\nu^2\delta_1^2}{K_{f1}^{\mathrm{IV}}}\right)\frac{d^2c_{b1}}{dx^2}, \quad (21a)$$

$$c_{b1}(-\infty) = 0, \qquad c_{b1}(0) = c_{s1}. \quad (21b)$$

Notice that Eqs. 1 and 2 at steady state are combined into one (Eq. 20 or 21) to simplify the solutions for the concentration waves. The feed port is located at $x = 0$. Note also that Eq. 20 or 21 is different from what has been used in the literature (Ruthven, 1983; Ching et al., 1985). The detailed mathematical derivation of these two equations can be found in the Appendix.

Instead of finite zone length boundary conditions (Ruthven, 1983; Kubota et al., 1989), the infinite zone length boundary conditions are used here, because (1) the analysis and results are simple so that the physical insights in the CMB system design are readily clear; and (2) in practice, high purity and recovery are desired; the operation conditions are designed to achieve small impurity concentrations at both raffinate and extract ports; that is, the concentrations of minor solutes at the two output ports should approach zero. Therefore, such boundary conditions are good approximations, as confirmed by the simulation results introduced later. By integrating Eqs. 20 and 21 with the specified boundary conditions, the following equations can be derived:

$$\frac{c_{b2}|_{x=0}}{c_{b2}|_{x=L^{\mathrm{I}}}} = \exp\left[\frac{(1+P\delta_2)\nu - u_0^{\mathrm{I}}}{E_{b2}^{\mathrm{I}} + \dfrac{P\nu^2\delta_2^2}{K_{f2}^{\mathrm{I}}}}L^{\mathrm{I}}\right] \quad (22)$$

$$\frac{c_{b1}|_{x=0}}{c_{b1}|_{x=-L^{\mathrm{IV}}}} = \exp\left[\frac{u_0^{\mathrm{IV}} - (1+P\delta_1)\nu}{E_{b1}^{\mathrm{IV}} + \dfrac{P\nu^2\delta_1^2}{K_{f1}^{\mathrm{IV}}}}L^{\mathrm{IV}}\right]. \quad (23)$$

Notice that if the linear velocities are determined from Eqs. 14 to 18, the lefthand side terms of Eqs. 20a and 21a vanish. These velocities will give linear concentration profiles at steady state instead of the exponential profiles given in Eqs. 22 and 23. Note that the linear concentration profiles are special case solutions. These profiles are used to benchmark the numerical algorithm and the simulation program described later.

Equations 22 and 23 can be rearranged to give the following:

$$u_\nu^{\mathrm{I}} \equiv (1+P\delta_2)\nu - u_0^{\mathrm{I}} = \beta_2^{\mathrm{I}}\left(\frac{E_{b2}^{\mathrm{I}}}{L^{\mathrm{I}}} + \frac{P\nu^2\delta_2^2}{K_{f2}^{\mathrm{I}}L^{\mathrm{I}}}\right) \quad (24)$$

$$u_\nu^{\mathrm{IV}} \equiv (1+P\delta_1)\nu - u_0^{\mathrm{IV}} = -\beta_1^{\mathrm{IV}}\left(\frac{E_{b1}^{\mathrm{IV}}}{L^{\mathrm{IV}}} + \frac{P\nu^2\delta_1^2}{K_{f1}^{\mathrm{IV}}L^{\mathrm{IV}}}\right) \quad (25)$$

where

$$\beta_2^{\mathrm{I}} \equiv \ln\left(\frac{c_{b2}|_{x=0}}{c_{b2}|_{x=L^{\mathrm{I}}}}\right) \quad (26)$$

$$\beta_1^{\mathrm{IV}} \equiv \ln\left(\frac{c_{b1}|_{x=0}}{c_{b1}|_{x=-L^{\mathrm{IV}}}}\right). \quad (27)$$

Note that β defines the ratio of the highest concentration to the lowest concentration of the standing wave. For example, β_2^{I} is the natural algorithm of the ratio of the concentration at the feed port to that at the raffinate port for solute 2. The higher the concentration ratios, the higher the product purities (from now on, for the sake of simplicity, β and product purity are used interchangeably). Note also that the lefthand side of Eqs. 24 and 25 correspond to the standing wave conditions in Eqs. 14 and 17. Equations 24 and 25 indicate that the modification of the linear velocities and bed moving velocity is related to axial dispersion and mass-transfer coefficients, zone lengths, and product purities. Similar results for solute 1 in zone II and for solute 2 in zone III can de derived to ensure that the concentrations of both solutes at the solvent port are restricted to prevent cross contaminations. Now the complete solutions of the linear velocities for the four zones can be found from the following five equations, Eqs. 28 to 32, if a feed flow rate is given, or Eqs. 28 to 31 and Eq. 33, if solvent flow rate is given

$$u_\nu^{\mathrm{I}} \equiv (1+P\delta_2)\nu - u_0^{\mathrm{I}} = \beta_2^{\mathrm{I}}\left(\frac{E_{b2}^{\mathrm{I}}}{L^{\mathrm{I}}} + \frac{P\nu^2\delta_2^2}{K_{f2}^{\mathrm{I}}L^{\mathrm{I}}}\right) \quad (28)$$

$$u_\nu^{\mathrm{II}} \equiv (1+P\delta_1)\nu - u_0^{\mathrm{II}} = \beta_1^{\mathrm{II}}\left(\frac{E_{b1}^{\mathrm{II}}}{L^{\mathrm{II}}} + \frac{P\nu^2\delta_1^2}{K_{f1}^{\mathrm{II}}L^{\mathrm{II}}}\right) \quad (29)$$

$$u_\nu^{\mathrm{III}} \equiv (1+P\delta_2)\nu - u_0^{\mathrm{III}} = -\beta_2^{\mathrm{III}}\left(\frac{E_{b2}^{\mathrm{III}}}{L^{\mathrm{III}}} + \frac{P\nu^2\delta_2^2}{K_{f2}^{\mathrm{III}}L^{\mathrm{III}}}\right) \quad (30)$$

$$u_\nu^{\mathrm{IV}} \equiv (1+P\delta_1)\nu - u_0^{\mathrm{IV}} = -\beta_1^{\mathrm{IV}}\left(\frac{E_{b1}}{L^{\mathrm{IV}}} + \frac{P\nu^2\delta_1^2}{K_{f1}^{\mathrm{IV}}L^{\mathrm{IV}}}\right) \quad (31)$$

$$\frac{F^{\text{feed}}}{\epsilon_b S} = u_0^{\text{I}} - u_0^{\text{IV}} \tag{32}$$

$$\frac{F^{\text{solv}}}{\epsilon_b S} = u_0^{\text{III}} - u_0^{\text{II}}. \tag{33}$$

Note that the β values can be different from zone to zone. Equations 28, 31 and 32 give the following relation between ν and the F^{feed}.

$$\left(\frac{P\beta_2^{\text{I}}\delta_2^2}{K_{f2}^{\text{I}}L^{\text{I}}} + \frac{P\beta_1^{\text{IV}}\delta_1^2}{K_{f1}^{\text{IV}}L^{\text{IV}}}\right)\nu^2 - P(\delta_2 - \delta_1)\nu + \frac{F^{\text{feed}}}{\epsilon_b S} + \frac{\beta_2^{\text{I}}E_{b2}^{\text{I}}}{L^{\text{I}}} + \frac{\beta_1^{\text{IV}}E_{b1}^{\text{IV}}}{L^{\text{IV}}} = 0. \tag{34}$$

Similarly, the relation of ν to the solvent flow rate can be expressed as

$$\left(\frac{P\beta_2^{\text{II}}\delta_2^2}{K_{f2}^{\text{II}}L^{\text{II}}} + \frac{P\beta_1^{\text{III}}\delta_1^2}{K_{f1}^{\text{III}}L^{\text{III}}}\right)\nu^2 + P(\delta_2 - \delta_1)\nu - \frac{F^{\text{solv}}}{\epsilon_b S} + \frac{\beta_2^{\text{II}}E_{b2}^{\text{II}}}{L^{\text{II}}} + \frac{\beta_1^{\text{III}}E_{b1}^{\text{III}}}{L^{\text{III}}} = 0. \tag{35}$$

If product purity and recovery are specified for a given system, there are five equations with five unknowns, indicating that closed-form solutions can be found for the four linear velocities and the bed movement velocity. Equations 28 to 32 define the standing-wave conditions when both E_b and K_f are significant. Also, Eqs. 28 to 31 and 34 define the maximum linear velocities for zones I and II and the minimum linear velocities for zones III and IV for a linear isotherm system. Any lower linear velocities for zones I and II and higher linear velocities for zones III and IV result in better than specified product purity and recovery, but with lower product concentrations. It is worth emphasizing that when axial dispersion and mass-transfer resistance are significant, the linear velocities and bed velocity calculated from Eqs. 28 to 32 give the highest throughput and lowest solvent consumption if the desired product purities (β^{I} and β^{II}) and the feed flow rate (F^{feed}) are specified for a given system.

Before any detailed analysis of Eqs. 28 to 35, the following observations can be made: (1) for a fixed u_0 in each zone; β is proportional to the Peclet number; $Pe = Lu_0/E_b$; and a number similar to the Stanton number, $St = K_f L/\nu$ (ν instead of u_0 is the characteristic velocity); (2) linear velocities can be found by fixing either the feed flow rate ν or the makeup solvent flow rate; (3) for a given feed flow rate, Eqs. 28 to 35 give the minimum solvent (desorbent) flow rate, or for a given solvent flow rate Eqs. 28 to 35 give the maximum feed flow rate that guarantees the specified β values.

When only axial dispersion is dominant and the other mass-transfer resistances are negligible ($K_f \to \infty$), the following are derived:

$$u_\nu^{\text{I}} \equiv (1 + P\delta_2)\nu - u_0^{\text{I}} = \beta_2^{\text{I}}\frac{E_{b2}^{\text{I}}}{L^{\text{I}}} \tag{36}$$

$$u_\nu^{\text{II}} \equiv (1 + P\delta_1)\nu - u_0^{\text{II}} = \beta_1^{\text{II}}\frac{E_{b1}^{\text{II}}}{L^{\text{II}}} \tag{37}$$

$$u_\nu^{\text{III}} \equiv (1 + P\delta_2)\nu - u_0^{\text{III}} = -\beta_2^{\text{III}}\frac{E_{b2}^{\text{III}}}{L^{\text{III}}} \tag{38}$$

$$u_\nu^{\text{IV}} \equiv (1 + P\delta_1)\nu - u_0^{\text{IV}} = -\beta_1^{\text{IV}}\frac{E_{b1}^{\text{IV}}}{L^{\text{IV}}}. \tag{39}$$

For a fixed feed flow rate, ν can be derived as:

$$\nu = \left(\frac{F^{\text{feed}}}{\epsilon_b S} + \beta_2^{\text{I}}\frac{E_{b2}^{\text{I}}}{L^{\text{I}}} + \beta_1^{\text{IV}}\frac{E_{b1}^{\text{IV}}}{L^{\text{IV}}}\right)/[P(\delta_2 - \delta_1)] \tag{40}$$

and the solvent flow rate becomes

$$\frac{F^{\text{solv}}}{\epsilon_b S} = P(\delta_2 - \delta_1)\nu + \frac{\beta_2^{\text{II}}E_{b2}^{\text{II}}}{L^{\text{II}}} + \frac{\beta_1^{\text{II}}E_{b1}^{\text{III}}}{L^{\text{III}}}. \tag{41}$$

Equations 36 and 39 suggest a linear relation between u_0 and ν (Figure 2a). For a fixed feed flow rate, the smaller the $\beta E_b/L$, the smaller the ν and u_0 (compare case (a) with case (b) in Figure 2a). If either E_b or β is increased or the zone

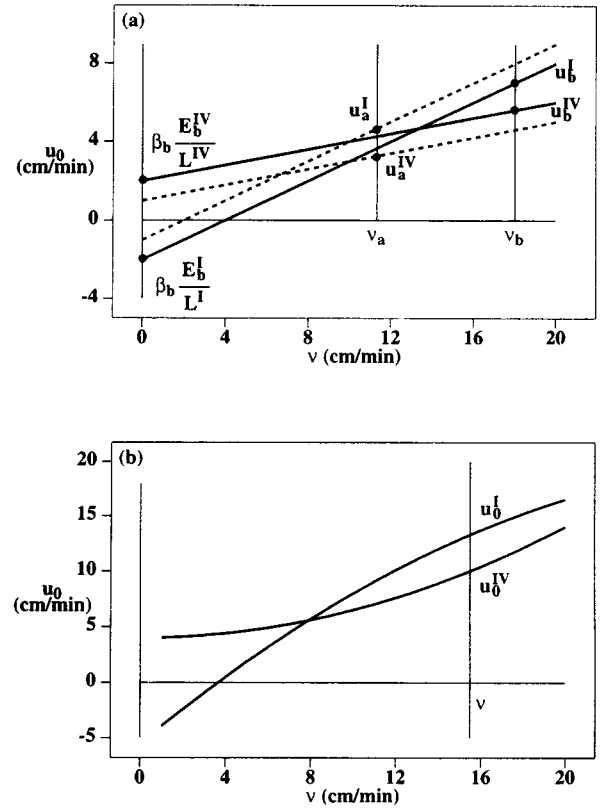

Figure 2. Relations between the linear velocities in zones I and IV (u_0^{I}, u_0^{IV}) and the bed movement velocity (ν).

Axial dispersion controls: dashed lines for small $\beta E_b/L$ [case (a)]; solid lines for large $\beta E_b/L$ [case (b)]. For the same feed flow rate, case (a) has a smaller ν than case (b); (b) both E_b and K_f dominant. For fixed E_b, β, L^{I}, and L^{IV}, the maximum feed flow rate is indicated by the thin line.

length is decreased, u_0 and ν have to be increased (solid lines vs. dashed lines). Therefore, virtually any value of β can be realized as long as the linear velocities are unlimited. Of course, in practice the linear velocities are limited by column pressure drop.

In practice, when large particles are used, both K_f and E_b can be dominant. Therefore, Eq. 34 has to be solved for the bed velocity as follows:

$$\nu = \frac{P(\alpha-1) \pm \sqrt{P^2(\alpha-1)^2 - 4\left(\frac{P\beta_2^{\mathrm{I}}\alpha^2}{K_{f2}^{\mathrm{I}}L^{\mathrm{I}}} + \frac{P\beta_1^{\mathrm{IV}}}{K_{f1}^{\mathrm{IV}}L^{\mathrm{IV}}}\right)\left(\frac{F^{\mathrm{feed}}}{\epsilon_b S} + \frac{\beta_2^{\mathrm{I}}E_{b2}^{\mathrm{I}}}{L^{\mathrm{I}}} + \frac{\beta_1^{\mathrm{IV}}E_{b1}^{\mathrm{IV}}}{L^{\mathrm{IV}}}\right)}}{2\delta_1\left(\frac{P\beta_2^{\mathrm{I}}\alpha^2}{K_{f2}^{\mathrm{I}}L^{\mathrm{I}}} + \frac{P\beta_1^{\mathrm{IV}}}{K_{f1}^{\mathrm{IV}}L^{\mathrm{IV}}}\right)}, \quad (42)$$

For systems with finite K_f and E_b, Eqs. 28 and 31 indicate that u_0 is a nonlinear function of ν (Figure 2b). For fixed E_b, K_f, β, and zone lengths, there exists a maximum feed flow rate (indicated by the thin line in Figure 2b). By contrast, Figure 2a shows that feed flow rate can be increased while maintaining the specified purities as long as ν and u_0 are increased accordingly.

Note that $u_\nu^{\mathrm{I}} > 0$, $u_\nu^{\mathrm{II}} > 0$, $u_\nu^{\mathrm{III}} < 0$, and $u_\nu^{\mathrm{IV}} < 0$ are not zeros, as in Eqs. 14 to 17. This is because the linear velocities in zones I and II have to be decreased to counterbalance the solute movement due to axial dispersion in order to keep solute 2 from reaching the raffinate port and solute 1 from reaching the desorbent port. Similarly, the linear velocities in zones III and IV have to be increased in order to prevent solute 1 from reaching the extract port and solute 2 from reaching the solvent port. The changes in the linear velocities are related to the product purity and recovery, axial dispersion coefficient, and individual zone length.

According to Eqs. 37 and 38, the linear velocity in zone II can be as low as zero and that in zone III can be as high as the system allows. This implies that if solvent recycle is not needed, zone II can be omitted, which results in the three-zone design used in many studies (Ching et al., 1992; Barker and Deeble, 1975).

Equations 28 to 31 also indicate that for fixed values of β and E_b, when u_ν approaches zero, L approaches infinity or E_b approaches zero, implying that if the linear velocities from Eqs. 14 to 19 are used, either the zone lengths have to be infinitely long or the system has to have negligible axial dispersion in order to achieve high purity and recovery at steady state. This can be explained from another view point. At steady state the solute concentrations at the output ports depend on E_b and K_f and are limited by those in the feed (as shown in Figures 3 to 7). If the zone lengths are finite and the raffinate concentration of solute 1 is less than that of the feed, the extract concentration of solute 1 has to be greater than zero due to component mass balance. Thus, the extract purity is limited. For similar reasons, the raffinate purity is also limited. In general, the product purities are always limited if the flow rates and bed velocity are obtained from Eqs. 14 to 19. In contrast, if Eqs. 28 to 31 are used, the linear velocities are adjusted according to E_b, K_f, L, and β such that the concentration of solute 1 at the extract port and that of solute 2 at the raffinate port can asymptotically approach zero, resulting in high product purities.

where $\alpha = \delta_2/\delta_1$. For a fixed feed flow rate, if zone linear velocities are limited (usually because of limited column pressure drop), so is ν (Eqs. 28 to 31). In order to have small ν, large δ_1 is needed. However, a system with large δ_1 takes a long time to reach steady state.

In order to have a physically meaningful solution for ν, β_1^{I} and β_2^{IV} must satisfy the following condition:

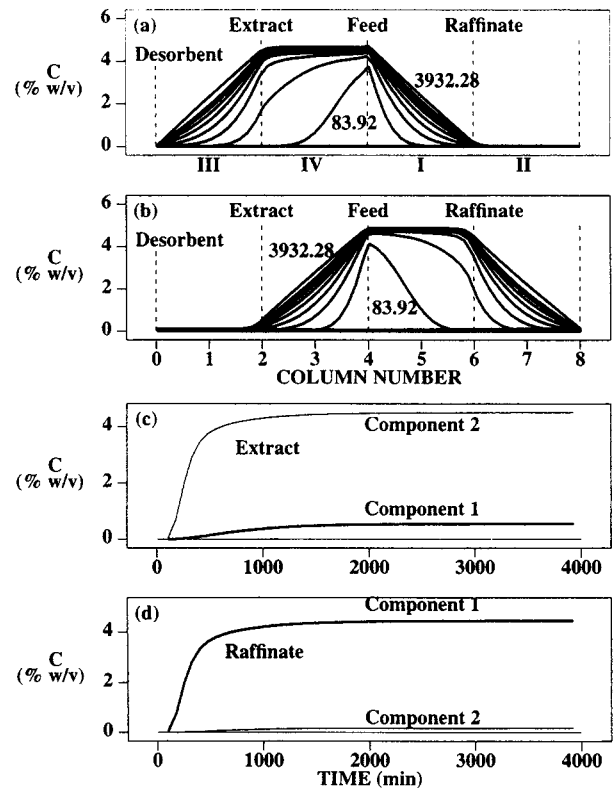

Figure 3. Simulation results for a CMB system.

The simulation parameters are listed in Table 4 except $E_b = 3.852\ \mathrm{cm^2 \cdot min^{-1}}$ and $K_{f1} = 50\ \mathrm{min^{-1}}$. (a) Column profiles for solute 2 at 167.32-min interval and 3,932.28 min for the one with the highest concentration. (b) Column profiles for solute 1. (c) Transient elution history at extract port. (d) Transient elution history profiles at raffinate port. The column numbers are given in (b) to facilitate comparison with corresponding SMB systems.

$$P(\alpha-1)^2-4\left(\frac{\beta_2^{\mathrm{I}}\alpha^2}{K_{f2}^{\mathrm{I}}L^{\mathrm{I}}}+\frac{\beta_1^{\mathrm{IV}}}{K_{f1}^{\mathrm{IV}}L^{\mathrm{IV}}}\right)\times\left(\frac{F^{\mathrm{feed}}}{\epsilon_b S}+\frac{\beta_2^{\mathrm{I}}E_{b2}^{\mathrm{I}}}{L^{\mathrm{I}}}+\frac{\beta_1^{\mathrm{IV}}E_{b1}^{\mathrm{IV}}}{L^{\mathrm{IV}}}\right)\geq 0. \quad (43)$$

Note that the equality gives the largest β_1 and β_2 values for a fixed feed flow rate or the largest feed flow rate for fixed β values. It is easily seen that when K_f is finite, there is a trade-off between the feed flow rate and the product purities. In other words, lowering feed flow results in higher product purity and vice versa. In contrast, when only axial dispersion is considered (Eqs. 36 to 40) virtually any product purity can be achieved by increasing the linear velocities (Figures 2a and 2b). Note also that the highest feed flow rate for fixed β values or the highest product purities for a fixed feed flow rate can be determined from the equality of Eq. 43.

When $\beta_1^{\mathrm{I}}=\beta_2^{\mathrm{IV}}=\beta$, $K_{f1}^{\mathrm{I}}=K_{f2}^{\mathrm{IV}}=K_f$, $L^{\mathrm{I}}=L^{\mathrm{IV}}=L$, and $E_{b2}^{\mathrm{I}}=E_{b1}^{\mathrm{IV}}=E_b$, Eq. 43 can be simplified and the maximum feed flow rate per bed volume (or throughput) can be found from the following :

$$P(\alpha-1)^2-4\beta\left(\frac{\alpha^2+1}{K_f}\right)\left(\frac{F^{\mathrm{feed}}}{\epsilon_b SL}+\frac{2\beta E_b}{L^2}\right)\geq 0. \quad (44)$$

Note that SL is the total bed volume in zone I or IV. Therefore, Eq. 44 indicates that if E_b does not change significantly with flow rate, for a fixed product purity and sorbent amount in zones I and IV, the longer the zone length, the higher the throughput. The practical implication is that as long as the column pressure drop does not exceed the system limit, long zones benefit system throughput. Also, the larger the selectivity α, the larger the throughput.

Because there is a trade-off between the feed flow rate and the product purity, the maximum β achievable for a system can be found for the following condition: $F^{\mathrm{feed}}=0$,

$$\beta\leq\sqrt{\frac{PK_fL^2}{8E_b}\left(1-\frac{2\alpha}{\alpha^2+1}\right)}. \quad (45a)$$

In practice, the feed flow rate has to be as high as possible in order to maximize throughput. Thus, Eq. 43 or 44 has to be used for the determination of the product purity and recovery. *Note, however, that the significance of Eq. 45a lies in its usefulness as a measure of the highest purity that can be achieved in a given system.* Note also that large L or large α results in high β values.

The lumped mass-transfer coefficient K_f can be related to the intraparticle diffusion coefficient, D_p, and the film mass-transfer coefficient, k_f (explained in the next section):

$$\beta\leq\frac{L}{2\sqrt{6}}\sqrt{\frac{P}{E_b}\left(1-\frac{2\alpha}{1+\alpha^2}\right)\Big/\left(\frac{R^2}{5\epsilon_p D_p}+\frac{R}{k_f}\right)}. \quad (45b)$$

Keep in mind that β is directly related to the product purity and recovery. The larger the β value, the higher the product purity and recovery. Equations 45a and 45b show a linear proportionality of the zone length to the β value. In practice, the gain of the purity and recovery by increasing zone length may not be as optimistic as shown in Eq. 45a or 45b. Increases in zone length usually result in increases in column numbers. Consequently, extracolumn dispersion can become significant and result in decreases in product purity and recovery. Equation 45b also shows that decreasing particle size is effective in increasing product purity. However, this is limited by the column pressure drop in a given system.

In summary, when the axial dispersion and the lumped mass-transfer resistance are negligible, Eqs. 14 to 17 and 19 define the maximum flow rates for zones I and II and minimum flow rates for zones III and IV that guarantee separation for a given feed flow rate. When both the axial dispersion and the mass-transfer resistance are dominant, the zone flow rates given in Eqs. 14 to 17 and 19 have to be modified. The flow rates in zones I and II have to be decreased and those in zones III and IV have to be increased to keep solute 2 from reaching the raffinate port and solute 1 from reaching the extract port. For a given system with a fixed feed flow rate, Eqs. 28 to 31 and 42 give the maximum flow rates for zones I and II and minimum flow rates for zones III and IV that guarantee separation with the specified purities. Note that for a given system with specified purities Eq. 43 gives the maximum feed flow rate for a fixed configuration. Most importantly, Eq. 43 indicates that for a specific system, the higher the feed flow rate, the lower the product purity and recovery and vice versa. For a fixed amount of sorbent Eq. 44 gives the highest feed flow rate that a system can operate; the longer the zone, the higher the system throughput. Equation 45 gives the highest product purity and recovery a system can achieve at zero feed flow rate. Furthermore, the higher the selectivity, the higher the throughput per bed volume, and the higher the product purity. In systems where only axial dispersion dominates, high product purity and recovery can be achieved by high zone and bed velocities (Figure 2a). However, when both E_b and K_f are dominant, the linear velocities are limited for a given purity and recovery (Figure 2b).

Lumped mass-transfer model for numerical simulation

In the following analysis, numerical simulations are used to test the simple and basic solutions obtained for CMB systems. A lumped mass-transfer model is employed here for simplicity, fast implementation, and fast simulation. The simulation results are used to validate the assumptions made in deriving the analytical solutions for CMB systems and further to investigate the applicability of these solutions to the design of SMB systems.

Mass Balance Equations for an Individual Column in SMB. The following mass balance equations are proposed for the individual columns within a zone in SMB (Figure 1a). For the mobile phase,

$$\frac{\partial c_{bi}}{\partial t}+u_0^{\mathrm{I}}\frac{\partial c_{bi}}{\partial x}=E_{bi}^{\mathrm{I}}\frac{\partial^2 c_{bi}}{\partial x^2}-PK_{fi}^{\mathrm{I}}(c_{bi}-c_i^*). \quad (46)$$

For the pore phase,

$$\epsilon_p^{\mathrm{I}} \frac{\partial c_i^*}{\partial t} + \left(1 - \epsilon_p^{\mathrm{I}}\right) \frac{\partial q_i}{\partial t} = K_{fi}^{\mathrm{I}}(c_{bi} - c_i^*), \qquad i = 1, 2, \ldots, N, \tag{47}$$

where N is the number of components. The boundary conditions for an individual column are

$$\left.\frac{\partial c_{bi}}{\partial x}\right|_{x=0} = \frac{u_0^{\mathrm{I}}}{E_{bi}^{\mathrm{I}}}\left[c_{bi} - c_{fi}(x,t)\right] \tag{48a}$$

$$\left.\frac{\partial c_{bi}}{\partial x}\right|_{x=L_{c_j}} = 0 \tag{48b}$$

where c_b is the bulk phase concentration; c_i^* is the average pore phase concentration; and q_i is the solid phase concentration; $c_{fi}(x,t)$ is the time-dependent output concentration from the mixer located in front of the jth column, u_0^{I} is the interstitial linear velocity; E_{bi}^{I} is the axial diffusion coefficient for the ith component in zone I; and K_{fi}^{I} is the lumped mass transfer coefficient, which can be found through the following analysis. In this study zero volume mixing is assumed in between columns within a zone. For cases with nonzero volume mixing (i.e., the volume of the connection tubing is taken into account) the conditions by Ramkrishna and Amundson (1974) should be used.

Correlation for Lumped Mass-Transfer Coefficient. For a linear isotherm, the solutions of the first- and the second-order central moment for a pulse input in a fixed bed can be derived as follows (Van Deemter et al., 1956; Ma and Guiochon, 1991):

$$\sigma_t^2 = 2t_0\left[\frac{E_b}{u_0^2}(1 + P\delta_i)^2 + \frac{P\delta_i^2}{K_f}\right] + \frac{t_p^2}{12}, \tag{49}$$

where t_p is the injection time and

$$t_0 = \frac{L_c}{u_0}. \tag{50}$$

The second-order central moment for a more detailed rate model with intraparticle diffusion can be found as (Kubin, 1965; Schneider and Smith, 1968; Ma et al., 1996)

$$\sigma_t^2 = 2t_0\left[\frac{E_b(1 + P\delta_i)^2}{u_0^2} + P\delta_i^2\left(\frac{R^2}{15\epsilon_p D_p} + \frac{R}{3k_f}\right)\right] + \frac{t_p^2}{12}. \tag{51}$$

Therefore, by equating the second-order central moments from the lumped model to that of the detailed rate model, the following relation between the lumped mass-transfer coefficient and the film mass transfer and intraparticle diffusion coefficients can be derived:

$$\frac{1}{K_f} = \frac{R^2}{15\epsilon_p D_p} + \frac{R}{3k_f}. \tag{52}$$

A similar relation can be found in Glueckauf (1955) and Santacesaria et al. (1982). Equation 52 can be used to estimate the lumped mass-transfer coefficient K_f from the pore diffusion coefficient, D_p; film mass-transfer coefficient, k_f; particle size, R; and particle porosity, ϵ_p. The values of E_b, D_p, and k_f can be obtained either from systematic fixed bed experiments or from correlations in the literature. The pore diffusion and film mass-transfer coefficients, for example, can be estimated from the Mackie–Meares correlation (1955) and the Wilson and Geankoplis correlation (1966), respectively. The axial dispersion coefficient can be estimated from the Chung and Wen correlation (1968).

Numerical Algorithm for SMB Systems

The SMB system shown in Figure 1a consists of four zones with $\{m^{\mathrm{I}}, m^{\mathrm{II}}, m^{\mathrm{III}}, m^{\mathrm{IV}}\}$ number of columns described by Eqs. 46 to 48. Each zone is operated at its own flow rate. Under the assumption of zero volume mixing in between columns, the c_{fi} in Eq. 48a for each zone takes the following values,

in between zones I and IV,

$$c_{fi}(L_+^{\mathrm{I}}, t) = \left[F^{\mathrm{IV}}c(L_-^{\mathrm{IV}}, t) + F^{\mathrm{feed}}c_{fi}\right]/F^{\mathrm{I}}, \tag{53a}$$

zones I and II,

$$c_{fi}(L_+^{\mathrm{II}}, t) = c(L_-^{\mathrm{I}}, t), \tag{53b}$$

zones II and III

$$c_{fi}(L_+^{\mathrm{III}}, t) = F^{\mathrm{II}}c(L_-^{\mathrm{II}}, t)/F^{\mathrm{III}}, \tag{53c}$$

zones III and IV

$$c_{fi}(L_+^{\mathrm{IV}}, t) = c(L_-^{\mathrm{III}}, t). \tag{53d}$$

At the time of port switching, the columns located upstream are shifted downstream into the adjacent zone for all four zones. This operation can be characterized as below:

$$c_{bi}(x,t) = \begin{cases} c_{bi}(x + jL_c, t), & t = nt_s \\ 0, & t = 0 \end{cases} \tag{54a}$$

$$c_i^*(x,t) = \begin{cases} c_i^*(x + jL_c, t), & t = nt_s \\ 0, & t = 0 \end{cases} \tag{54b}$$

$$q_i(x,t) = \begin{cases} q_i(x + jL_c, t), & t = nt_s \\ 0, & t = 0, \end{cases} \tag{54c}$$

$$i = 1, 2, \ldots, N$$

$$j = 1, 2, \ldots, \{m^{\mathrm{I}}, m^{\mathrm{II}}, m^{\mathrm{III}}, m^{\mathrm{IV}}\}$$

$$n = 1, 2, \ldots, \infty,$$

where n is the number of switches; $t_s = L_c/v$ is the time between switching; and L_c is the column length. Furthermore, when the column length is infinitesimally small (approaching the element width for numerical solution) the preceding algorithm can be used to simulate CMB systems. This is how the

computer program is coded so that both SMB and CMB simulations can be performed by one program and the results can be compared. Note that the algorithm presented here is entirely different from directly solving Eqs. 1 and 2 numerically. The latter approach is limited to CMB only and cannot generate the results for SMB systems; in SMB the steady-state effluent concentrations are cyclic, whereas in CMB the steady-state effluent concentrations are constants.

Method of numerical simulation

Any numerical-simulation algorithm introduces errors in the solution. The accuracy of a simulation algorithm is crucial to the studies of diffusion-controlled processes (Ma et al., 1996), because the errors introduced by some simulation algorithms can have dispersion effects on the concentration waves that are not due to physical processes but due to numerical dispersion (Lin et al., 1989). Therefore, higher than second-order accuracy is required for any numerical-simulation algorithm. The method of orthogonal collocation on finite elements (OCFE) is proven to have such accuracy (Ma and Guiochon, 1991; Finlayson, 1980; Yu and Wang, 1989) and is used in this study.

In solving Eqs. 46 to 48 under the constraints of Eqs. 53 to 54, the individual columns are divided into thin elements; on each element orthogonal polynomials are used for each component to interpolate the concentration profiles; in between two adjacent elements, the continuity condition,

$$\left.\frac{\partial c_{bi}}{\partial x}\right|_{x=\Delta x_{(j+1)}} = \left.\frac{\partial c_{bi}}{\partial x}\right|_{x=\Delta x_j}$$

is enforced (Finlayson, 1980). In SMB mode, the boundary conditions, Eqs. 48a and 48b, are enforced in between each column in addition to the preceding concentration flux continuity condition in between columns where there is no input or output port. In CMB mode, the boundary conditions, Eqs. 48a and 48b, are only enforced at the input and output port positions. Convergence of the solutions is tested by increasing the element number and decreasing the integration time until no differences between solutions from different runs are observable and the mass balances are satisfied. In this study, individual component mass balance is within 1%, that is, the difference between the output rate and the input rate of a solute is within 1%. The most difficult run (4,000 min in simulated experimental run time) requires 26 h CPU time on an HP 715/100 workstation with 128 MB of memory. Accuracy in component mass balance can be improved to better than 1%. However, a much longer CPU time is required.

Results and Discussion

First, the second-order central moments of elution peaks are used to benchmark simulation results from fixed-bed operations. The simulated steady-state concentration profiles of CMB systems are then compared with the theoretical profiles for systems operated under zone flow and bed velocities (1) derived without considering axial dispersion and mass-transfer effects; (2) derived with finite-axial and mass-transfer coefficients. Also, simulation results from CMB systems are compared with those from SMB systems under the conditions that the flow rates are the same in both systems and the bed movement velocity (ν) in CMB is equal to the time-averaged port movement velocity in SMB, L_c/t_s. The two key points of this study are the following: (1) for SMB with a large number of columns, despite the periodic movement of the concentration waves in SMB, the average raffinate and extract product concentrations within one cycle approach those of CMB; (2) the conditions that can achieve standing waves in CMB can be applied to design SMB systems as long as ν in a CMB system is equal to L_c/t_s in a SMB system. These are checked with detailed SMB simulations below. Finally, simulations are compared with experimental data from the literature (Ching et al., 1991).

Benchmark of simulations using second-order moment and limiting case solutions

Two steps are taken to check the program coding and to benchmark the simulation results: (1) moment analysis is used to check the accuracy of the simulation in fixed-bed mode; (2) simulation results are compared with those predicted from theoretical analysis for CMB systems; specifically, the linear concentration profiles predicted from the theoretical analysis of Eqs. 20 and 21. The first step is to ensure the accuracy of the simulation code used in this study for CMB and SMB systems; the OCFE numerical method for each column (Eqs. 46 to 48) in fixed-bed operation mode has been benchmarked previously (Ma and Guiochon, 1991). The second step is to check if the simulation algorithm proposed for SMB systems gives results that approach those of CMB systems when the number of columns increases.

Table 1 shows the benchmark of the second-order central moments in fixed-bed mode. Good agreements are obtained between those from the theoretical calculations and those from the effluent concentrations at the raffinate port. Similar results (not shown here) are obtained for effluent concentrations at the extract port. This indicates that the program is working properly if port switching is not activated. If the bed moves as it should in CMB systems, there are no solutions similar to those of the moment analysis. But at steady state when u_ν is zero, the linear concentration profiles predicted from the analysis of Eqs. 20 to 23 over a large range of E_b and K_f can be used to check whether the simulations give the expected linear profiles. In the figures presented in the next section, the simulation results obtained with different values of E_b, K_f, and L show that indeed the standing waves are straight lines as predicted from the theoretical analysis. The results in these figures also show that the numerical algorithm (Eqs. 46, 47 and 53 to 54) for SMB does indeed give simulation results that approach those of CMB (Eqs. 1 and 2) as the number of subdivisions in each zone increases.

Simulation results using the flow rates obtained from equilibrium analysis

In this section, the effects of axial dispersion, mass-transfer resistance, and zone length on steady-state concentration profiles are studied for systems designed according to the equilibrium analysis (Eqs. 14 to 18). The simulation parameters are similar to those in the literature (Ching et al., 1991).

Effect of Axial Dispersion in CMB Systems. Figure 3a shows the transient concentration profiles for the more retained

Table 1. System and Numerical Parameters Used in Simulation Program Benchmark in Fixed-bed Mode

System Parameters	F 5.80	Length (cm) 95	ϵ_b 0.45	ϵ_p 0.50	ID (cm) 1.40	R (μm) 11
Feed Concentrations	C_{f1} (% w/v) 20.0		C_{f2} (% w/v) 20.0		Pulse Time	t_p (min) 0.001
Simulation Parameters	Δx (cm) 2.375			Colloc. No. 3		Δt (min) 0.001*
Component	E_b (cm$^2\cdot$min^{-1})			K_f (min^{-1})		Equilibrium: K
1	3.8515			50		0.12
2	3.8515			50		0.38
	σ_{t1}^2		σ_{t2}^2		t_{r1}	t_{r2}
Eqs. 49 and 50	3.7114		4.5004		19.1122	20.9150
Simulation	3.7314		4.5246		19.1639	20.9716
Component	E_b (cm$^2\cdot$min^{-1})			K_f (min^{-1})		Equilibrium: K
1	3.8515			1		0.12
2	3.8515			1		0.38
	σ_{t1}^2		σ_{t2}^2		t_{r1}	t_{r2}
Eqs. 49 and 50	12.2353		17.4411		19.1122	20.9150
Simulation	12.2867		17.5116		19.1690	20.9767

*All the combinations of 0.001 or 0.01 as integration time and 20 or 40 as element number give the same results. Note in this study, the units are: minute for time, centimeter for length, and millimeter for volume.

component at every 167.32 min, starting at 83.92 min, with the last one at 3,932.28 min. Figure 3b shows the same results as in Figure 3a for the less retained component. The elution history profiles at the extract port are shown in Figure 3c, and those at the raffinate port in Figure 3d. They still show slight increases at 4,000 min and the standing concentration waves are nearly straight lines, indicating that the system is approaching steady state (Figures 3c and 3d).

Figure 4 shows the comparison of simulation results with $K_f = 50$ and two E_b values, 1.2224 (thin line) and 3.852 (thick line). The concentration profiles are significantly different with these E_b values, indicating that axial dispersion is important in this system. Note that the standing waves for the

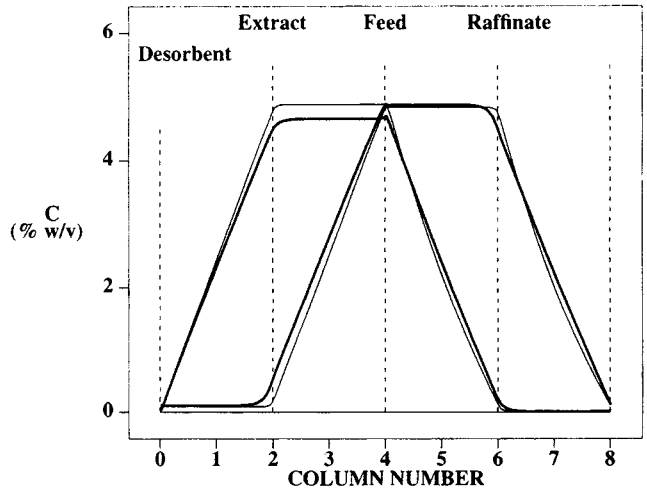

Figure 4. Effects of E_b on the steady-state concentration profiles in a CMB system (run time, 4,000 min).

The parameters are listed in Table 4, except the following: thick lines, $E_b = 3.852$ cm$^2\cdot$min^{-1}, $K_f = 50$ min^{-1}; thin lines, $E_b = 1.222$ cm$^2\cdot$min^{-1}, $K_f = 50$ min^{-1}.

run with $E_b = 1.2224$ are not as straight as those with $E_b = 3.852$. In this case, both runs ended at 4,000 min; the difference between the profiles indicates that steady states have not yet been reached for the system with smaller E_b.

Effect of Lumped Mass Transfer in CMB Systems. In Figure 5, the thick lines were obtained with $E_b = 3.852$ and $K_f = 50$, whereas the thin lines were obtained with E_b being kept the same but K_f being reduced from 50 to 10. Although the differences between the concentration profiles are small, the product purities of both raffinate and extract are improved when K_f is increased (Table 2). Figure 6 compares the effects of K_f at a smaller E_b than that in Figure 5. K_f changes from 10 (thick lines) to 1 (thin lines). There are significant differences in the concentrations profiles, indicating that both E_b and K_f are important. The standing waves are still straight lines, indicating the concentration profiles are approaching steady state.

Table 2. Simulation Results from Equilibrium Analysis

	Col. No.	E_b	K_f	Purity (R)	Purity (E)
CMB(4-4-4-4)	80-80-80-80*	3.852	10	97.599%	93.545%
CMB(3-3-3-3)	60-60-60-60	3.852	10	96.780%	91.855%
CMB(2-2-2-2)	40-40-40-40	3.852	10	95.027%	88.171%
CMB	40-40-40-40	3.852	50	96.249%	89.187%
CMB	40-40-40-40	3.852	150	96.460%	89.379%
CMB	40-40-40-40	1.222	50	98.045%	96.281%
CMB	40-40-40-40	1.222	1	77.428%	80.243%
SMB	3-3-3-3**	3.852	10	88.855%	88.409%
SMB	2-2-2-2	3.852	10	85.678%	85.958%
SMB	2-2-2-2	3.852	50	87.263%	87.181%
SMB	2-2-2-2	3.852	150	87.525%	87.388%
SMB	2-2-2-2	1.222	50	94.258%	95.511%
SMB	2-2-2-2	1.222	1	73.344%	79.312%

*The number of elements in Zone I to IV.
**The division number here equals the number of columns in Zone I to IV. Each column is divided into 20 elements. For a 4,000-min run of the 2-2-2-2 configuration, CPU time is about 13 h on HP 715/100 workstations. All the flow rates and other simulation conditions are the same as in Table 4 except the E_b and K_f values.

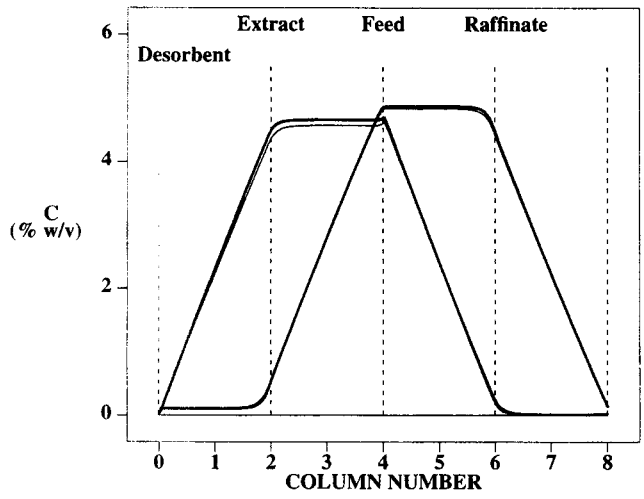

Figure 5. Effects of K_f on the steady-state concentration profiles in a CMB system (run time, 4,000 min).

The parameters are listed in Table 4, except: thick lines, $E_b = 3.852$ cm^2·min^{-1}, $K_f = 50$ min^{-1}; thin lines, $E_b = 3.852$ cm^2·min^{-1}, $K_f = 10$ min^{-1}.

Effect of Zone Length in CMB Systems. Figure 7 shows the effect of zone length on the steady-state concentration profiles. The axis is labeled with the number of columns for the convenience of reference to the experimental system introduced later. Again the standing waves are approaching straight lines in all three cases with different zone lengths. The slopes of the concentration profiles change with changing zone length. The ratios of the concentrations at the feed port to that at the raffinate port for solute 1 and to that at the extract port for solute 2 are similar for all three different zone lengths. The three simulations differ largely in the transient times. It takes a long time for a system with long zones

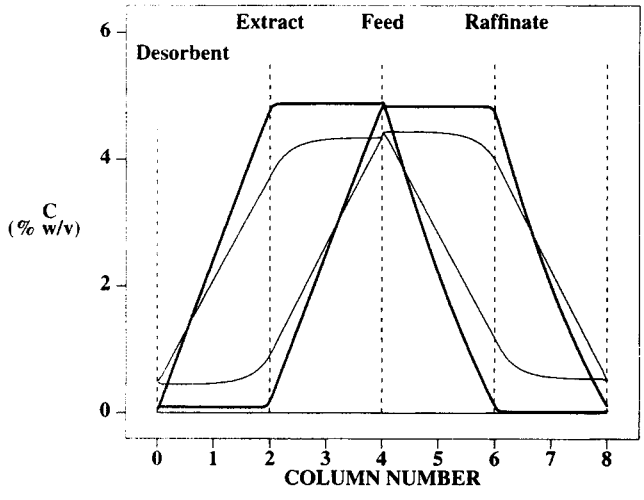

Figure 6. Effects of K_f on the steady-state concentration profiles in a CMB system (run time, 4,000 min).

The parameters are listed in Table 4, except: thick lines, $E_b = 1.222$ cm^2·min^{-1}, $K_f = 50$ min^{-1}; thin lines, $E_b = 1.222$ cm^2·min^{-1}, $K_f = 1$ min^{-1}.

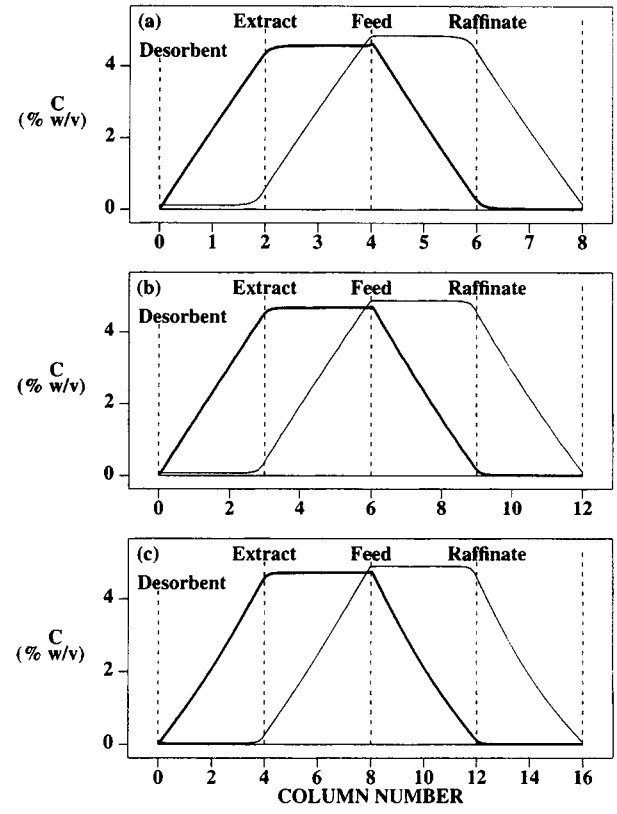

Figure 7. Effects of zone length on the steady-state concentration profiles in a CMB system.

The parameters are listed in Table 4, except: $E_b = 1.222$ cm^2·min^{-1}, $K_f = 10$ min^{-1}; (a) zone length, 95 cm (40 elements); (b) zone length, 142.5 cm (60 elements); (c) zone length, 190 cm (80 elements).

to reach steady state. This is why the standing waves are not quite straight lines in Figure 7c, even though the run time is three times that in Figure 7b.

Note from Eqs. 28 to 31, decreasing E_b has a similar effect as increasing zone length, that is, when E_b is small, a system needs more time for the standing waves to become straight lines than one with a larger E_b, as shown in Figure 4. This is because the development of the standing wave of the minority species in systems with small E_b is slow compared to that in systems with large E_b. Similarly, systems with a large K_f have a longer transient time.

Comparison of CMB with SMB Systems. Figures 8–10 compare the simulation results of CMB systems with those of SMB systems with different combinations of E_b and K_f values. Note that concentration profiles in SMB are not stationary within a cycle (in between port switching). Here the SMB profiles at midcycles are compared with those of CMB. One can see that the steady-state concentration profiles from CMB systems are significantly different from those obtained from SMB systems. Especially, when E_b is large, the concentration waves are straight lines in CMB systems, whereas in SMB systems significant deviation from straight lines are observed. However, such differences diminish when E_b is small, or K_f is large, or the number columns is increased (Hadajat et al., 1986). Furthermore, if the design is based on finite E_b and

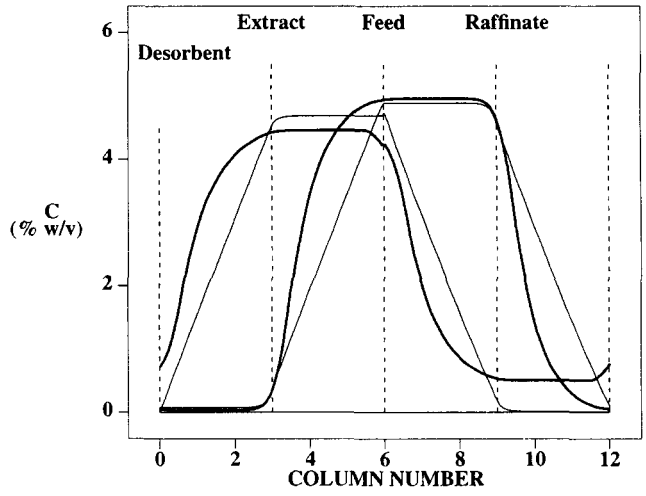

Figure 8. Steady-state concentration profiles: CMB vs. SMB systems (run time, 4,000 min).

The parameters are listed in Table 4 except $E_b = 3.852$ cm^2·min^{-1}, $K_f = 10$ min^{-1}; thin lines, CMB; thick lines, SMB.

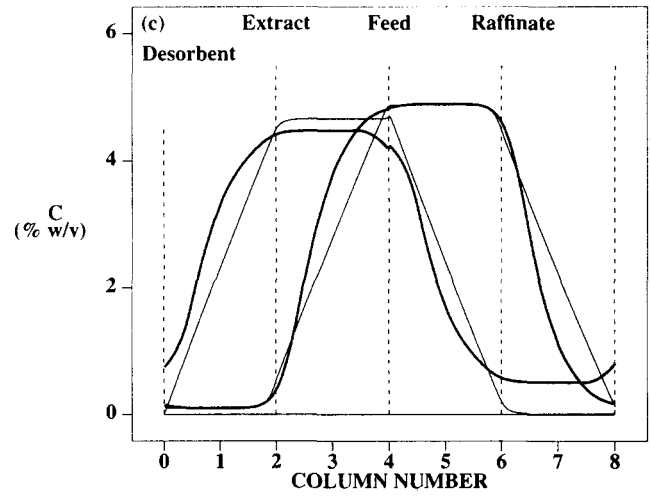

Figure 10. Comparison of the steady-state concentration profiles from CMB and SMB systems (run time, 4,000 min).

The parameters are listed in Table 4 except $E_b = 3.852$ cm^2·min^{-1}, $K_f = 50$ min^{-1}; thin lines, CMB; thick lines, SMB.

K_f analysis, the differences become much smaller and the product purities become much closer, as will be shown next.

Simulation results using flow rates derived from nonequilibrium analysis (finite E_b and K_f)

In this section, systems with different E_b, K_f, and L are simulated. The operational parameters are derived from Eqs. 28 to 31 and 42. The purpose is to see the performances of a system operated under the parameters derived from Eqs. 28 to 31 and 42.

CMB Systems with Different E_b. Figure 11 compares the simulation results for CMB systems with two different axial dispersion coefficients (thick lines: $E_b = 1.222$, thin lines: $E_b = 3.852$). In order to achieve the same product purity, flow rates and bed velocities are chosen according to E_b, K_f, and zone lengths (Eqs. 28 to 31 and 42); they are different for these two cases, as listed in the figure captions. The values of β_1 and β_2 are the same and equal to 4.6052, respectively. The corresponding concentration ratio is 100, as listed in Table 3. One can easily see that the shape of the concentration profiles in Figure 11 are similar, except the solute concentrations at the feed-port position for the thick lines are lower than those of the thin lines. This is because the flow rates for the thick lines are larger than those for the thin lines as a result of the larger E_b value (Eqs. 28 to 31). Note that all four β values from the simulation profiles are close to the given values within simulation accuracy. Note also that the purity of the extract is not the same as that of the raffinate, because concentration profiles for the two solutes are not identical. The same β value results in different concentrations at the output ports, thus different product purities.

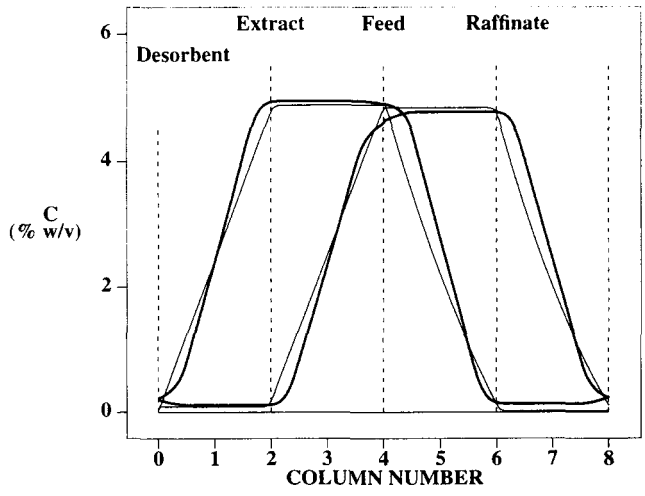

Figure 9. Steady-state concentration profiles: CMB vs. SMB systems (run time, 4,000 min).

The parameters are listed in Table 4 except $E_b = 1.222$ cm^2·min^{-1}, $K_f = 50$ min^{-1}; thin lines, CMB; thick lines, SMB.

Table 3. Simulation Results with Finite E_b and K_f $\beta_1 = \beta_2 = 4.6052$*

	Col. No.	E_b	K_f	Purity (R)	Purity (E)
CMB(3-3-3-3)	60-60-60-60	3.852	10	99.772%	99.844%
CMB(2-2-2-2)	40-40-40-40	3.852	10	99.463%	99.852%
CMB	40-40-40-40	1.222	10	99.539%	99.923%
CMB	40-40-40-40	1.222	50	99.896%	99.876%
CMB	60-60-60-60	1.222	50	99.955%	99.936%
SMB	2-2-2-2	3.852	10	98.028%	99.586%
SMB	2-2-2-2	1.222	10	98.433%	99.742%
SMB	2-2-2-2	1.222	50	99.129%	99.616%
SMB	1-1-1-1*	1.222	50	93.810%	96.371%
SMB	1-1-1-1**	3.852	10	92.579%	96.966%
SMB	2-2-2-2	3.852	50	98.782%	99.144%
SMB	3-3-3-3	3.852	10	98.959%	99.568%
SMB	3-3-3-3	3.852	50	99.059%	99.076%

*The concentration ratio defined in Eqs. 26 and 27 is 100.
**The column length is twice that of other runs, and 40 elements are used for each column. The same convention as in Table 2 is used here.

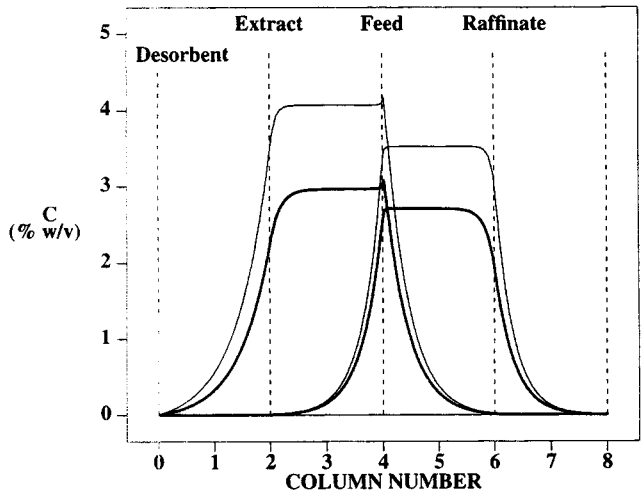

Figure 11. Effects of E_b on the steady-state concentration profiles in a CMB system (run time, 4,000 min).

Equations 28 to 31 and 42 are used to calculate the flow rates and the bed moving velocity. The parameters are listed in Table 4 except thin lines, $E_b = 1.222$ cm$^2\cdot$min^{-1}, $K_f = 10$ min^{-1}, $\nu = 6.5010$ cm$\cdot$min^{-1}, $F^{\mathrm{I}} = 8.1776$ mL$\cdot$min^{-1}, $F^{\mathrm{II}} = 7.4656$ mL$\cdot$min^{-1}, $F^{\mathrm{III}} = 8.39867$ mL$\cdot$min^{-1}, $F^{\mathrm{IV}} = 7.7058$ mL$\cdot$min^{-1}; thick lines, $E_b = 3.852$ cm$^2\cdot$min^{-1}, $K_f = 10$ min^{-1}, $\nu = 9.5851$ cm$\cdot$min^{-1}, $F^{\mathrm{I}} = 11.931$ mL$\cdot$min^{-1}, $F^{\mathrm{II}} = 10.877$ mL$\cdot$min^{-1}, $F^{\mathrm{III}} = 12.487$ mL$\cdot$min^{-1}, $F^{\mathrm{IV}} = 11.492$ mL$\cdot$min^{-1}.

CMB Systems with Different K_f. The effects of K_f on the concentration profiles, shown in Figure 12, are similar to those observed in Figure 11. The purities are listed in Table 3. Notice that the product purities for the profiles in the thick lines and the thin lines are similar (Table 3), whereas the purities in Figures 5a and 5b are largely different (Table 2). This indicates that when the mass-transfer effects are considered in the nonequilibrium design, the effect of zone subdivision is reduced.

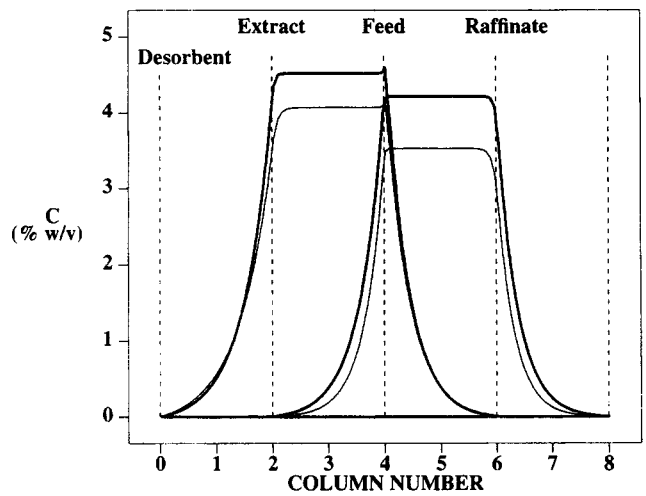

Figure 12. Effects of K_f on the steady-state concentration profiles in a CMB system (run time, 4,000 min).

Equations 28 to 31 and 42 are used to calculate the flow rates and the bed moving velocity. The parameters are listed in Table 4 except thin lines, the same as thin lines in Figure 11; thick lines, $E_b = 1.222$ cm$^2\cdot$min^{-1}, $K_f = 50$ min^{-1}, $\nu = 5.4302$ cm$\cdot$min^{-1}, $F^{\mathrm{I}} = 6.8813$ mL$\cdot$min^{-1}, $F^{\mathrm{II}} = 6.2871$ mL$\cdot$min^{-1}, $F^{\mathrm{III}} = 6.9825$ mL$\cdot$min^{-1}, $F^{\mathrm{IV}} = 6.3852$ mL$\cdot$min^{-1}.

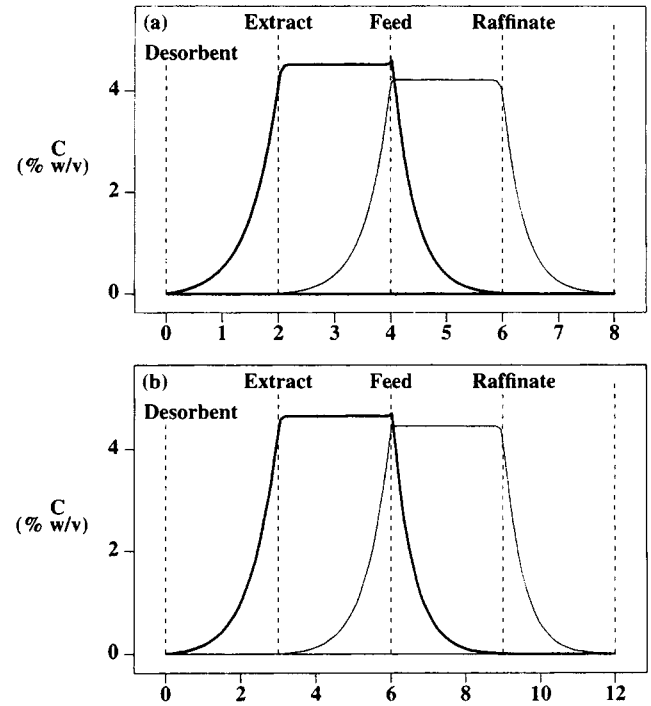

Figure 13. Effects of zone length on the steady-state concentration profiles in a CMB system (run time, 4,000 min).

Equations 28 to 31 and 42 are used to calculate the flow rates and the bed moving velocity. The parameters are listed in Table 4 except $E_b = 1.222$ cm$^2\cdot$min^{-1}, $K_f = 50$ min^{-1}; (a) the same as the thick lines in Figure 12; (b) zone length: 142.5 cm (60 elements), $\nu = 5.1215$ cm$\cdot$min^{-1}, $F^{\mathrm{I}} = 6.5056$ mL$\cdot$min^{-1}, $F^{\mathrm{II}} = 5.9443$ mL$\cdot$min^{-1}, $F^{\mathrm{III}} = 6.5717$ mL$\cdot$min^{-1}, $F^{\mathrm{IV}} = 6.0079$ mL$\cdot$min^{-1}.

CMB Systems with Different Zone Lengths. Figure 13 shows the concentration profiles obtained at different zone lengths. Note that the flow rates for Figure 13a are different from those for Figure 13b. Despite the difference in flow rates, the β values obtained from the simulations are close to those used in the analytical solutions within simulation accuracy. The product purities are slightly different (Table 3) because the concentration profiles are different. In contrast, the product purities in the equilibrium design in Figures 9a, 9b and 9c are significantly different (Table 2). Again this is because the effect of subdivision is reduced in the nonequilibrium design.

Comparison of Simulations of CMB and SMB Systems. Figure 14 compares the midcycle SMB profiles with CMB profiles. The differences in concentration profiles in Figure 14 are not as great as in Figure 8. The purities obtained with CMB simulations significantly differ from those with SMB simulations, as in Table 2, but such differences are much smaller in Table 3 than in Table 2. Keep in mind that a CMB system corresponds to an SMB system with an infinite number of columns. The large contrast in purities between Tables 2 and 3 shows that the number of divisions does not have a

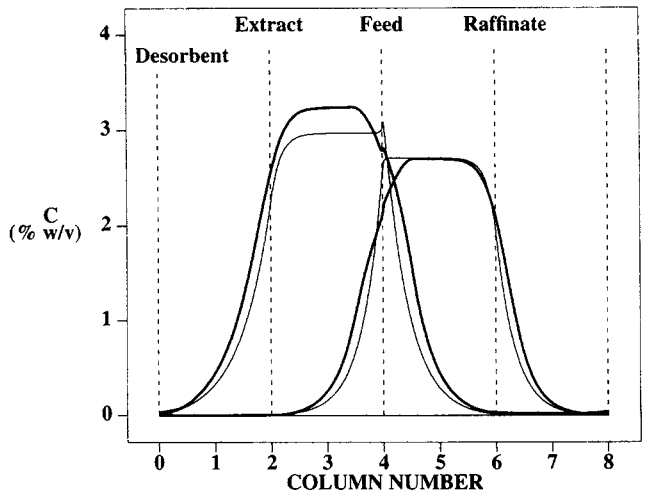

Figure 14. Simulations for CMB and SMB systems (run time, 4,000 min).

Equations 28 to 31 and 42 are used to calculate the flow rates and the bed moving velocity. The parameters are listed in Table 4, except: $E_b = 3.852\ \text{cm}^2 \cdot \text{min}^{-1}$, $K_f = 10\ \text{min}^{-1}$; thick lines: $t_s = 4.9556$ min, flow rates same as those for the thick lines in Figure 11; thin lines: the same as thick lines in Figure 11.

strong effect on the product purities in systems operated with flow rates and bed velocity obtained from the nonequilibrium design (Eqs. 28 to 31 and 42), whereas the effects of zone subdivisions are significant if the flow rates and bed velocity are determined from the equilibrium design (Eqs. 14 to 17 and 19). The practical implication is that as few as four columns in an SMB system can be used to obtain high-purity products if high-efficiency columns are used and the flow rates and port switching time are properly determined. In Table 3, the comparison of product purities between systems with eight and four columns and the same zone length shows that eight column divisions is sufficient for high-purity requirement. With four columns the purities can be higher than those shown in Table 3 if a β value larger than 4.6052 is used in deriving the zone flow rates and the bed velocity. However, more diluted products result, because feed flow rate is decreased and the solvent flow rate is increased.

Comparison of SMB simulation with experimental data from the literature

In this section, a linear isotherm system for fructose and raffinose separation (Ching et al., 1991) is studied. Because the model in this study is different from that in the original report, the original parameters have to be converted to values suitable for this study. The two models differ in the isotherm parameter definition and the lumped mass-transfer coefficients. In the original report, the adsorbed solute concentrations used in defining the isotherm and mass-transfer parameters were based on per-particle volume, whereas those used in this study are based on per-solid volume within sorbent particles. The equilibrium capacity from the particle volume basis, q_p, can be related to that from the solid volume basis, q_s, by the following equation:

$$q_p V_p = q_s(1-\epsilon_p)V_p + c\epsilon_p V_p, \tag{55}$$

where ϵ_p is the intraparticle void fraction and V_p is the particle volume. Equation 55 basically states that to get the adsorbed concentration based on the solid volume, q_s, the amount in the particle void has to be explicitly accounted for. For the lumped mass-transfer coefficients, we have,

$$\begin{aligned} K_p(q_p^{eq} - q_p^*) &= K_p\{\epsilon_p c_b + (1-\epsilon_p)Kc_b \\ &\quad - [\epsilon_p c^* + (1-\epsilon_p)Kc^*]\} \\ &= K_p[\epsilon_p + (1-\epsilon_p)K](c_b - c^*), \end{aligned}$$

where $q_p^{eq} = Kc_b$ are the concentrations when the bulk phase and the pore phase are in equilibrium and $q_p^* = Kc^*$ are the actual concentrations when the two phases are not in equilibrium. Therefore, the lumped mass transfer coefficient (K_f) in this study is related to that (K_p) in the original report by the following equation:

$$K_f = K_p[\epsilon_p + (1-\epsilon_p)K]. \tag{56}$$

Note that Eqs. 55 and 56 apply only to linear isotherm systems.

Figure 15 compares the simulation results from the SMB simulation and the experimental data (experimental run 2) from Ching et al. (1991). The lines are the concentrations averaged over the cycle time, t_s. The concentration profiles are sampled at midcycle time. The simulation parameters derived here and listed in Table 4 are the same as those in the original study except the particle porosity, the isotherm parameters, and the lumped mass transfer parameters, which are converted from the original values using Eqs. 55 and 56. We see that the column profiles and the effluent concentration histories are well predicted.

Comparison Between CMB and SMB. Both column concentration profiles and the effluent history concentrations at the output ports at steady state and the transient state are important in comparing the performances of SMB and CMB processes to justify the applicability of conditions derived for CMB and SMB. Figure 16 shows such comparisons of CMB and SMB simulations for the same system as in Figure 15. The SMB effluent concentrations averaged over one port switching cycle, rather than the concentrations at the midcycle time in between two consecutive port switching cycles (Hotier, 1996), are compared with those from the CMB simulation. The simulated SMB concentration profiles, on the other hand, were obtained at the midcycle time as in Ching et al. (1985).

In Figure 16, there are small differences between CMB and SMB in the transient concentration effluent histories of major components at the output ports. However, the differences of the effluent concentration histories of the minor components at the output ports are large. This is because the solute concentrations at the solvent port position are higher in SMB than in CMB. They pass the solvent port and cause the contamination of the output concentrations with the minor components.

More simulations (not shown here) were conducted to investigate the transition from SMB to CMB mode. When the column number increases, the concentration effluent histories become smoother and less cyclic. The average effluent

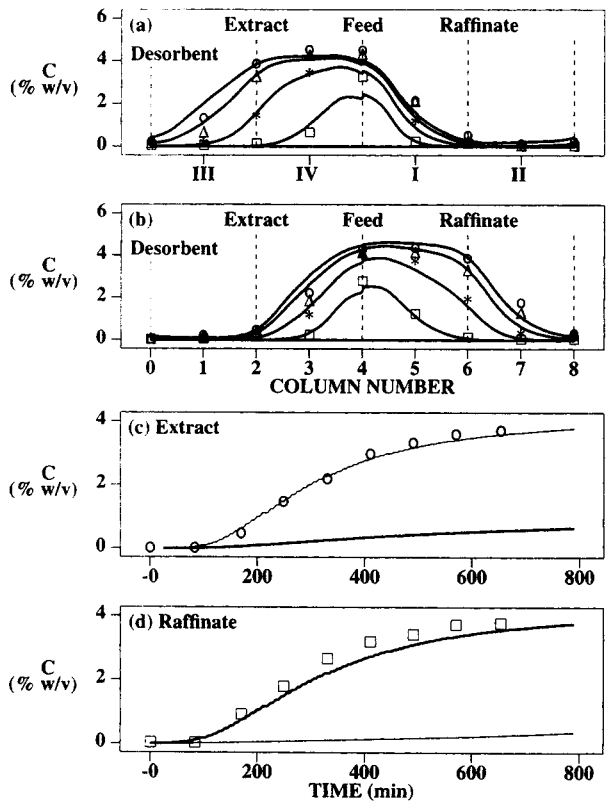

Figure 15. SMB simulation and experimental data from literature (Ching et al., 1991).

The simulation parameters are listed in Table 4. (a) Column profiles for fructose at 83.6 min (square), 250.8 min (star), 501.6 min (delta), 752.4 min (circle). (b) Column profiles for raffinose at 83.6 min (square), 250.8 min (star), 501.6 min (delta), 752.4 min (circle). Symbols are experimental data points; lines are simulation results. (c) Transient elution history at extract port. Symbols are experimental data points for fructose. The lines are the time-averaged concentrations over a switching cycle. (d) Transient elution history profiles at raffinate port. Same figure convention as that in (c).

concentration histories in SMB approach those in CMB. The differences in product purities between CMB and SMB become insignificant when the number of columns in SMB is sufficiently large (eight for this particular system) and the axial dispersion and mass-transfer effects are taken into account in determining the flow rates and port switching time.

Comparison Between Equilibrium and Nonequilibrium Designs. Notice that the operation conditions listed in Table 4 and in the original article are the same as those from the Eqs. 14 to 19. In order to compare the performances with operation conditions from the equilibrium analysis with those from the nonequilibrium analysis, simulations using the conditions from Eqs. 28 to 31 and 42 with $\beta = 3.6889$ for the four zones are conducted. The concentration profiles and the effluent histories (not shown here) are similar to those in Figure 15. The product purities are improved as follows, raffinate: from 92.167% to 95.436%; extract: from 80.774% to 98.914%. Note that to achieve higher product purities the feed flow rate has to be reduced from 0.5 mL·min^{-1} to 0.122 mL·min^{-1}, as required by Eq. 43. The solvent flow rate is increased from 0.5 mL·min^{-1} to 1.211 mL·min^{-1}. The extract and raffinate flow rates are 0.547 mL·min^{-1} and 0.786 mL·min^{-1}, respectively. The reduction in feed flow and the increase in solvent flow result in the decreases in the product concentrations. Note that the maximum β at zero feed flow rate (Eq. 45a) is 5.9775, a fairly low value. In order to have a

Table 4. System and Numerical Parameters Used in Simulation of Fructose–Raffinose Separation

	Zone I	Zone II	Zone III	Zone IV
E_b^* (cm^2/min)	3.852	3.808	3.852	3.808
K_{f1} (l/min)	2.6676	2.6676	2.6676	2.6676
K_{f2} (l/min)	4.6644	4.6644	4.6644	4.6644
L (cm)	95	95	95	95
F (mL·min^{-1})	5.8	5.3	5.8	5.3

Single Column	R (μm)	L_c (cm)	ϵ_b	ϵ_p	ID (cm)
	11	47.5	0.45	0.50	1.40

Equilibrium Constants	K_1^{**}	K_2^{**}
	0.12	0.38

Feed Concentrations	C_{f1} (% w/v)	C_{f2} (% w/v)
	5.0	5.0

Simulation Parameters	Δx (cm)	Colloc. No.	Δt (min)	Switching Time (min)
	2.375	3	0.05	10.45

Source: Ching et al. (1991).
*$E_b = 0.46 \times u_0$.
**The unit of the solid-phase concentration is per solid volume of stationary phase.

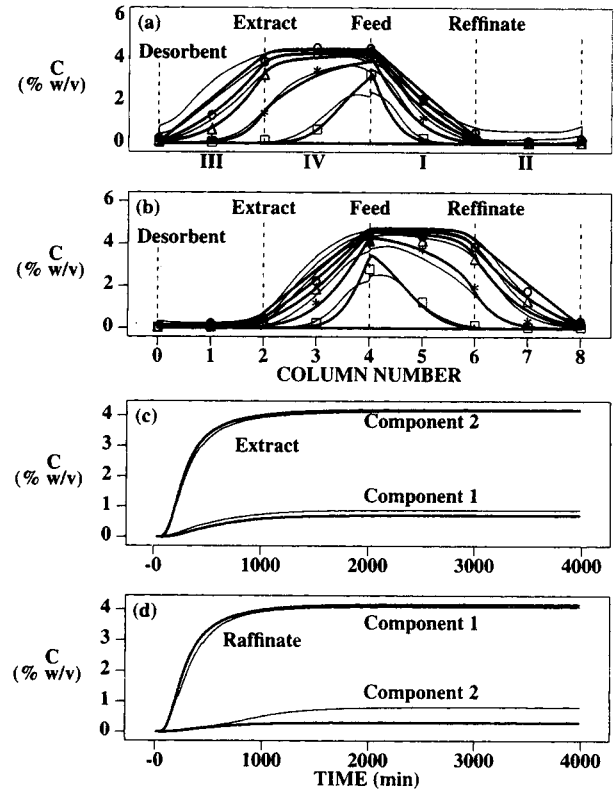

Figure 16. CMB (thick lines) and SMB (thin lines) simulations with experimental data (symbols) (the same figure convention and simulation parameters are used as in Figure 15).

reasonable throughput, that is, a finite feed flow rate, the desired β has to be much smaller than 5.9775.

To further improve product purities and throughput, longer zone lengths, smaller E_b, and larger K_f values are needed. For this particular system, increasing the column length may not be feasible with existing equipment, since the column is already long (45×1.4 cm) and there are eight such columns in the system. Besides, relatively small particles are used (22 μm in diameter). Note that the apparent E_b values estimated from the experimental data (Ching et al., 1991) are about 3.8 $cm^2 \cdot min^{-1}$. This apparent axial dispersion coefficient lumps the effects of both extracolumn dispersion and intracolumn axial dispersion. It is nearly 100 times larger than the E_b estimated using the Chung and Wen (1968) correlation for intracolumn dispersion. Therefore, extracolumn dispersions due to the void space in tubings and valves are controlling in this system, as noted in the original article. Decreasing extracolumn dispersion, if possible, can significantly increase throughput and product purities.

From Eqs. 28 to 31 and 42, another improvement that can be made using the given equipment is a new configuration, one column in zones II and III and three columns in zones I and IV (1-3-3-1). The maximum β is now 8.9663 for zones I and IV. Figure 17 shows the simulation results. In the simulation, all the β values are kept the same as 3.6889. As expected from Eq. 44, the feed flow is now 0.333 $mL \cdot min^{-1}$, which is much higher than 0.122 $mL \cdot min^{-1}$ in the previous configuration (2-2-2-2). The solvent flow rate is increased from 1.211 $mL \cdot min^{-1}$ to 1.996 $mL \cdot min^{-1}$. This is because the bed lengths in zones I and III are decreased, causing the increase in the zone flow rates, as expected from Eqs. 29 and 30. Note that the solvent to feed flow rate ratio is actually lower than in the previous configuration. The feed flow rate in this new configuration is lower than the feed flow rate in the original study, 0.5 $mL \cdot min^{-1}$. If feed flow rate higher than 0.5 $mL \cdot min^{-1}$ and product purities higher than 95% are desired, longer zone lengths will be needed. In this case, the equipment has to be redesigned in order to achieve both higher throughput and higher product purities.

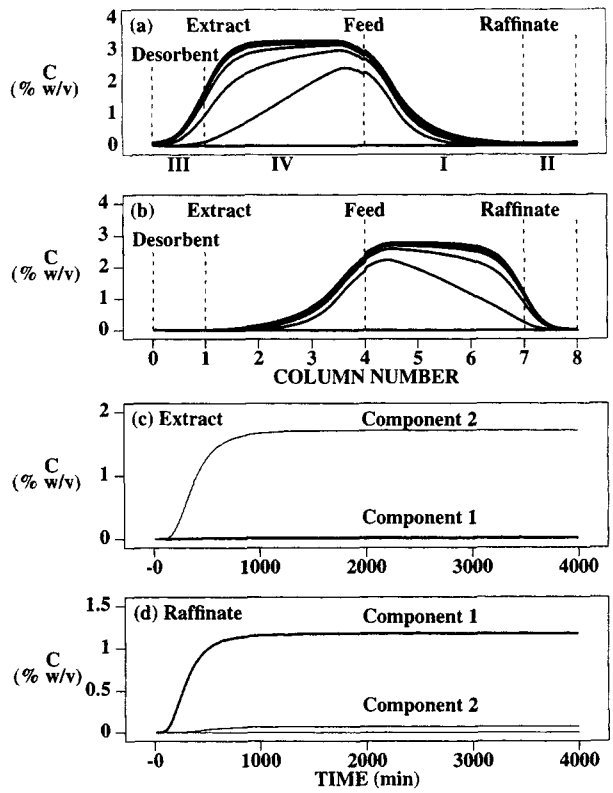

Figure 17. Concentration profiles and effluent histories for the improved design: zone I, 1 column; zone II, 3 columns; zone III, 3 columns; zone IV, 1 column (1-3-3-1).

Product purities are: extract 94.36%; raffinate: 98.97%. The same figure convention as in Figure 15 is used. Simulation parameters are the same as in Table 4, except: t_s = 6.7228 min, $F^{I} = 8.8413$ $mL \cdot min^{-1}$, $F^{II} = 7.4537$ $mL \cdot min^{-1}$, $F^{III} = 9.4499$ $mL \cdot min^{-1}$, $F^{IV} = 8.5079$ $mL \cdot min^{-1}$.

Conclusions

Design equations are derived from the standing wave analysis of CMB systems with linear isotherms. The equations explicitly link product purity to port switching time, flow rates, and zone and column lengths for systems with or without mass-transfer effects. Optimal interstitial and bed velocities can be found from these equations. If flow rates from the equilibrium analysis are used in a system with significant mass-transfer resistances, low product purity can result. However, for a fixed feed flow rate in a given system, the equilibrium design gives the lowest solvent consumption and the highest product concentrations. To achieve both high purity and high throughput, equations from the analysis with finite E_b and K_f have to be used for the determination of the flow rates and bed moving velocity. If axial dispersion is dominant, high product purity and high throughput can be achieved using high zone flow rates and a high bed velocity. If both axial disperison and film mass transfer and intraparticle diffusion are dominant, there exists a maximum product purity that a given system can achieve. There is a trade-off between the feed flow rate and the product purities; the higher the feed flow rate, the lower the product purities, and vice versa. There is also a trade-off between zone lengths and the feed flow rate for a fixed total bed volume; the longer the zone lengths, the higher the feed flow rate for given product purities. The larger the selectivity, the higher the throughput, and the higher the product purities. Large column-capacity factors result in low bed velocities, but a long transient time.

A numerical algorithm for the simulation of both SMB and CMB operations using a fixed-bed model is proposed. Simulation results are benchmarked with those predicted from theory. Comparison of CMB with SMB shows that port switching time and flow rates from standing wave analysis for CMB systems can be readily applied to SMB systems to achieve similar performances. When the flow rates and bed velocity are derived from the equilibrium analysis, the number of subdivisions in each zone strongly affect the product purity and recovery. However, when the flow rates and bed velocity are derived from the solutions that take into account axial dispersion and mass-transfer effects, the product purities of SMB are similar to those obtained from CMB, because the effects of subdivision are reduced.

Finally, the method developed here is used to analyze the separation of raffinose and fructose (Ching et al., 1991). Sim-

ulation results are in close agreement with the original experimental data. Both equilibrium analysis and nonequilibrium analysis are used to derive the flow rates and port switching time. The nonequilibrium analysis suggests that the same equipment configured differently and operated at different flow rates and switching times can achieve higher product purities or higher throughput.

Acknowledgments

This research was supported by grants from NSF (GER9024174), the Peterson Foundation, and Bristol-Myers Squibb Company. The authors are thankful to Mr. Ken Shultis from Bristol-Myers Squibb Company and Professor B. C. Lin from An Shan Iron and Steel Institute, China, for their helpful discussions and suggestions on this work.

Notation

F = volumetric flow rate
L = zone length
L_+ = column inlet position
L_- = column outlet position
S = column cross-section area
c_0 = bed initial concentration
c_f = feed bulk concentration
c_s = steady-state concentration
m = column number
q^{eq} = adsorbate concentration at equilibrium based on solid volume
t = time
t_0 = retention time of a nonadsorbing solute
t_p = injection time
u_0 = net interstitial linear velocity with respect to the feed port
$\bar{u}_0$ = interstitial linear velocity, Eq. 1
x = position inside the bed
Δx = elment width
α = relative retention factor
δ = retention factor, Eq. 3b
σ = second-order central moment

Superscripts and Subscripts

ext = extract port
raf = raffinate port
solv = solvent port
i = index
j = index
s = solute movement or steady state
t = time variant

Literature Cited

Adachi, S., "Simulated Moving-bed Chromatography for Continuous Separation of Two Components and Its Application to Bioreactors," *J. Chromatog. A*, **658**, 271 (1994).

Broughton, D. B., "Molex: Case History of a Process," *Chem. Eng. Prog.*, **64**, 60 (1968).

Broughton, D. B., R. W. Neuzil, J. M. Pharis, and C. S. Brearley, "The Parex Process for Recovering Paraxylene," *Chem. Eng. Prog.*, **66**, 70 (1970).

Charton, F., and R.-M. Nicoud, "Complete Design of a Simulated Moving Bed," *J. Chromatog. A*, **702**, 97 (1995).

Ching, C. B., K. H. Chu, K. Hidajat, and M. S. Uddin, "Experimental and Modeling Studies on the Transient Behavior of a Simulated Countercurrent Adsorber," *J. Chem. Eng. Jpn.*, **24**(5), 614 (1991).

Ching, C. B., and D. M. Ruthven, "An Experimental Study of a Simulated Counter-current Adsorption System: I. Isothermal Steady State Operation," *Chem. Eng. Sci.*, **40**, 877 (1985).

Ching, C. B., D. M. Ruthven, and K. Hidajat, "Experimental Study of a Simulated Counter-Current Adsorption System: III. Sorbex Operation," *Chem. Eng. Sci.*, **40**, 1411 (1985).

Ching, C. B., K. H. Chu, K. Hidajat, and D. M. Ruthven, "Experimental Study of a Simulated Counter-current Adsorption Systems: VII. Effects of Non-linear and Interacting Isotherms," *Chem. Eng. Sci.*, **48**, 1343 (1993).

Ching, C. B., K. H. Chu, K. Hidajat, and M. S. Uddin, "Comparative Study of Flow Schemes for a Simulated Countercurrent Adsorption Separation Process," *AIChE J.*, **38**, 1744 (1992).

Chu, K. H., and M. A. Hashim, "Simulated Countercurrent Adsorption Processes: A Comparison of Modeling Strategies," *Chem. Eng. J.*, **56**, 59 (1995).

Chung, S. F., and C. Y. Wen, "Longitudinal Dispersion of Liquid Flowing Through Fixed and Fluidized Beds," *AIChE J.*, **14**, 857 (1968).

Corbett, J., and D. Burke, "System Optimization in the Chromatographic Separation of Fructose from Dextrose in the Corn Wet Milling Industry," *Symp. on Industrial-Scale Process Chromatographic Separations*, New Orleans, March (1996).

deRosset, A. J., R. W. Neuzil, and D. J. Korous, "Liquid Column Chromatography as a Predictive Tool for Continuous Countercurrent Adsorptive Separations," *Ind. Eng. Chem. Des. Dev.*, **15**, 261 (1976).

Finlayson, B. A., *Nonlinear Analysis in Chemical Engineering*, McGraw-Hill, New York (1980).

Ganetsos, G., and P. E. Barker, eds., *Preparative and Production Scale Chromatography*, Marcel Dekker, New York (1993).

Glueckauf, E., *Ion-Exchange and Its Applications*, Society of Chemical Industry, London, p. 34 (1955).

Hashimoto, K., S. Adachi, H. Moujima, and Y. Ueda, "A New Process Combining Adsorption and Enzyme Reaction for Producing Higher-Fructose Syrup," *Biotech. Bioeng.*, **25**, 2371 (1983).

Hashimoto, K., S. Adachi, and Y. Shirai, "Continuous Desalting of Proteins with a Simulated Moving-bed Adsorber," *Agric. Biol. Chem.*, **52**, 2161 (1988).

Hidajat, K., C. B. Ching, and D. M. Ruthven, "Simulated Countercurrent Adsorption Processes: A Theoretical Analysis of the Effect of Subdividing the Adsorbent Bed," *Chem. Eng. Sci.*, **41**, 2953 (1986).

Hotier, G., "Physically Meaningful Modeling of the 3-Zone and 4-Zone Simulated Moving Bed Processes," *AIChE J.*, **42**, 154 (1996).

Kishihara, S., S. Fujii, H. Tamaki, K. B. Kim, N. Wakiuchi, and T. Yamamoto, "Continuous Chromatographic Separation of Sucrose, Glucose, and Fructose using a Simulated Moving-bed Adsorber," *Int. Sugar JNL*, **94**, 305 (1992).

Kubin, M., "Contribution to the Theory of Chromatography," *Collect. Czech. Chem. Commun.*, **30**, 1104 (1965).

Kubota, K., C. Hata, and S. Hayashi, "A Study of a Simulated Moving Bed Adsorber Based on the Axial Dispersion Model," *Can. J. Chem. Eng.*, **67**, 1025 (1989).

Lin, B. C., Ma, Z., and G. Guiochon, "Influence of Calculation Errors in the Numerical Simulation of Chromatographic Elution Band Profiles Using an Ideal or Semi-ideal Model," *J. Chromatog.*, **484**, 83 (1989).

Ma, Z., T. Mallmann, B. D. Burris, and N.-H. L. Wang, "SMB for Large-Scale Sugar Separations," submitted, *AIChE J.* (1997).

Ma, Z., and G. Guiochon, "Application of Orthogonal Collocation on Finite Elements in the Simulation of Non-linear Chromatography," *Comput. Chem. Eng.*, **15**, 415 (1991).

Ma, Z., R. D. Whitley, and N.-H. L. Wang, "Pore and Surface Diffusion in Multicomponent Adsorption and Liquid Chromatography Systems," *AIChE J.*, **42**, 1244 (1996).

Mackie, J. S., and P. Meares, "The Diffusion of Electrolytes in a Cation-exchange Resin Membrane," *Proc. Roy. Soc. London, Ser. A.*, **232**, 498 (1955).

Ramkrishna, D., and N. R. Amundson, "Stirred Pots, Tubular Reactors, and Self-Adjoint Operators," *Chem. Eng. Sci.*, **29**, 1353 (1974).

Rhee, H.-K., R. Aris, and N. R. Amundson, "Multicomponent Adsorption in Continuous Countercurrent Exchangers," *Phil. Trans. Roy. Soc. London A.*, **269** 187 (1971).

Ruthven, D., "The Axial Dispersed Plug Flow Model for Continuous Counter-Current Adsorbers," *Can. J. Chem. Eng.*, **61**, 881 (1989).

Ruthven, D., and C. B. Ching, "Counter-Current and Simulated

Counter-Current Adsorption Separation Processes," *Chem. Eng. Sci.*, **44**, 1011 (1989).
Santacesaria, E., M. Morbidelli, A. Servida, G. Storti, and S. Carra, "Separation of Xylenes on Y Zeolites. 2. Breakthrough Curves and Their Interpretation," *Ind. Eng. Chem. Process Des. Dev.*, **21**, 446 (1982).
Schneider, P., and J. Smith, "Chromatographic Study of Surface Diffusion," *AIChE J.*, **14**, 886 (1968).
Storti, G., M. Mazzotti, M. Morbidelli, and S. Carra, "Robust Design of Binary Countercurrent Adsorption Separation Processes," *AIChE J.*, **39**, 471 (1993).
Storti, G., R. Baicocchi, M. Mazzotti, and M. Morbidelli, "Design of Optimal Operating Conditions of Simulated Moving Bed Adsorptive Separation Units," *Ind. Eng. Chem. Res.*, **34**, 288 (1995).
Storti, G., M. Masi, S. Carra, and M. Morbidelli, "Optimal Design of Multicomponent Countercurrent Adsorption Separation Processes Involving Nonlinear Equilibria," *Chem. Eng. Sci.*, **44**, 1329 (1989).
Ulrich, P. E., and J. T. Hsu, "Study of Simulated Moving-Bed Separation Processes Using a Staged Model," *Ind. Eng. Chem. Res.*, **28**, 1211 (1989).
Van Deemter, J. J., F. J. Zuiderweg, and A. Klinkenberg, "Longitudinal Diffusion and Resistance to Mass Transfer as Causes of Nonideality in Chromatography," *Chem. Eng. Sci.*, **5**, 271 (1956).
Wankat, P. C., *Rate-Controlled Separations*, Blackie, Glasgow/London (1994).
Wilson, E. J., and C. J. Geankoplis, "Liquid Mass Transfer at Very Low Reynolds Numbers in Packed Beds," *Ind. Eng. Chem. Fundam.*, **5**, 9 (1966).
Yu, Q., and N.-H. L. Wang, "Computer Simulation of the Dynamics of Multicomponent Ion Exchange and Adsorption in Fixed Beds—Gradient Moving Finite Element Method," *Comput. Chem. Eng.*, **13**, 915 (1989).
Zhong, G., and G. Guiochon, "Analytical Solution for the Linear Ideal Model of Simulated Moving Bed Chromatography," *Chem. Eng. Sci.*, **51**, 4307 (1996).

Appendix: Derivation of Steady-State Equation with Finite E_b and K_f

When steady state is reached, the following can be derived from Eqs. 1 and 2:

$$E_{bi}\frac{d^2c_{bi}}{dx^2} = (u_0 - \nu)\frac{dc_{bi}}{dx} + PK_{fi}(c_{bi} - c_i^*) \tag{A1}$$

$$\nu\delta_i\frac{dc_i^*}{dx} = -K_{fi}(c_{bi} - c_i^*). \tag{A2}$$

Differentiation of both sides of Eq. A2 gives:

$$\nu\delta_i\frac{d^2c_i^*}{dx^2} = -K_{fi}\left(\frac{dc_{bi}}{dx} - \frac{dc_i^*}{dx}\right). \tag{A3}$$

Multiplying both sides of Eq. A3 by $\nu\delta_i$, gives,

$$(\nu\delta_i)^2\frac{d^2c_i^*}{dx^2} = -K_{fi}\left(\nu\delta_i\frac{dc_{bi}}{dx} - \nu\delta_i\frac{dc_i^*}{dx}\right). \tag{A4}$$

Rearranging Eq. A4 gives:

$$\frac{(\nu\delta_i)^2}{K_{fi}}\frac{d^2c_i^*}{dx^2} + \nu\delta_i\frac{dc_{bi}}{dx} = \nu\delta_i\frac{dc_i^*}{dx}. \tag{A5}$$

Eliminating the second term of the righhand side of Eq. A1 by substituting Eqs. A2 and A5 into A1, one has the following:

$$E_{bi}\frac{d^2c_{bi}}{dx^2} + (\nu - u_0)\frac{dc_{bi}}{dx} + P\frac{(\nu\delta_i)^2}{K_{fi}}\frac{d^2c_i^*}{dx^2} + P\nu\delta_i\frac{dc_{bi}}{dx} = 0. \tag{A6}$$

Note at the steady state, the mass-transfer rates, $PK_{fi}[c_{bi}(x) - c_i^*(x)]$, depend only on the difference of the local concentrations. The following is assumed to simplify Eq. A6:

$$\frac{d^2c_{bi}}{dx^2} = \frac{d^2c_i^*}{dx^2}. \tag{A7}$$

Therefore, Eq. A6 becomes

$$\left(E_{bi} + \frac{P\nu^2\delta_i^2}{K_{fi}}\right)\frac{d^2c_{bi}}{dx^2} + [(1 + P\delta_i)\nu - u_0]\frac{dc_{bi}}{dx} = 0. \tag{A8}$$

This is the steady-state equation for the system described in Eqs. 1 and 2.

In order to check the validity of Eq. A7, a second-order equation for $\Delta c_i = c_{bi} - c_i^*$ is derived. At the steady state, the following can be obtained from Eqs. A1 and A2:

$$\nu\delta_i E_{bi}\frac{d^2c_{bi}}{dx^2} = \nu\delta_i(u_0 - \nu)\frac{dc_{bi}}{dx} + \nu\delta_i PK_{fi}(c_{bi} - c_i^*) \tag{A9}$$

$$E_{bi}\nu\delta_i\frac{d^2c_i^*}{dx^2} = -E_{bi}K_{fi}\frac{d(c_{bi} - c_i^*)}{dx}. \tag{A10}$$

From Eqs. A2, A9, and A10, a second-order equation for Δc_i is derived as follows:

$$\nu\delta_i E_{bi}\frac{d^2(\Delta c_i)}{dx^2} = [E_{bi}K_{fi} + (u_0 - \nu)\delta_i\nu]\frac{d(\Delta c_i)}{dx} + K_{fi}[(1 + P\delta_i)\nu - u_0](\Delta c_i). \tag{A11}$$

The solution of Eq. A11 has the following form:

$$\Delta c_i = W_1 e^{r_+ x} + W_2 e^{r_- x}, \tag{A12}$$

where W_1 and W_2 are to be determined from the boundary conditions. The eigenvalues (r_+, r_-) can be derived as below:

$$r_\pm = \frac{E_{bi}K_{fi} + (u_0 - \nu)\delta_i\nu \pm \sqrt{[E_{bi}K_{fi} + (u_0 - \nu)\delta_i\nu]^2 + 4\nu\delta_i E_{bi}K_{fi}[(1+P\delta_i)\nu - u_0]}}{2\nu\delta_i E_{bi}} \tag{A13}$$

Note Δc_i should be finite even when x is large; therefore, W_1 should be zero in order to have a physically meaningful solution. Equation A12 becomes

$$\Delta c_i = W_2 e^{r_- x}. \tag{A14}$$

The solution r_- from Eq. A13 can be approximated by the following:

$$r_- \approx -\frac{K_{fi}[(1+P\delta_i)\nu - u_0]}{E_{bi}K_{fi} + (u_0 - \nu)\delta_i\nu} \tag{A15}$$

if

$$\left|\frac{4\nu\delta_i E_{bi}K_{fi}[(1+P\delta_i)\nu - u_0]}{[E_{bi}K_{fi} + (u_0 - \nu)\delta_i\nu]^2}\right| \ll 1. \tag{A16}$$

Equation A15 corresponds to the eigenvalue of the following first-order equation:

$$[E_{bi}K_{fi} + (u_0 - \nu)\delta_i\nu]\frac{d(\Delta c_i)}{dx} = -K_{fi}[(1+P\delta_i)\nu - u_0](\Delta c_i). \tag{A17}$$

Equation A16 and the Taylor expansion give

$$\sqrt{1 + \frac{4\nu\delta_i E_{bi}K_{fi}[(1+P\delta_i)\nu - u_0]}{[E_{bi}K_{fi} + (u_0 - \nu)\delta_i\nu]^2}} \approx 1 + \frac{2\nu\delta_i E_{bi}K_{fi}[(1+P\delta_i)\nu - u_0]}{[E_{bi}K_{fi} + (u_0 - \nu)\delta_i\nu]^2}. \tag{A18}$$

Equation A18 simplifies Eq. A13 to Eq. A15. One can see that Eq. A11 can be approximated by Eq. A17 if the condition in Eq. A16 is satisfied. Note this approximation is equivalent to

$$\frac{d^2(\Delta c_i)}{dx^2} = 0, \tag{A19}$$

which is the condition in Eq. A7.

Let's examine the validity of Eq. A16. The subscript i is dropped in the following for simplicity. Note that for the standing wave designs Eq. 28 is satisfied and can be used to simplify Eq. A16 to the following:

$$\frac{4\left(\frac{E_b}{K_f}\right)\left(\frac{\nu\delta}{K_f}\right)\left(\frac{\beta}{L}\right)}{\left[\left(\frac{E_b}{K_f}\right) + P\left(\frac{\nu\delta}{K_f}\right)^2\right]\left[1 - \left(\frac{\nu\delta}{K_f}\right)\left(\frac{\beta}{L}\right)\right]^2} \ll 1. \tag{A20}$$

Note also Eq. 42 is satistied for the standing wave designs. Therefore, Eq. A20 can be further simplified as

$$Y = \frac{\left(\frac{E_b}{K_f}\right)\left(\frac{\beta}{L}\right)^2\left(\frac{\alpha - 1}{1+\alpha^2}\right)}{\left[\left(\frac{E_b}{K_f}\right)\left(\frac{\beta}{L}\right)^2 + \frac{P}{4}\left(\frac{\alpha - 1}{1+\alpha^2}\right)^2\right]\left[1 - \frac{\alpha - 1}{2(1+\alpha^2)}\right]^2} \ll 1, \tag{A21}$$

where β/L can be found from Eq. 44 as follows:

$$\frac{\beta}{L} \le \frac{1}{2}\sqrt{\frac{K_f}{E_b}}\left[\sqrt{B^2 + \frac{P(\alpha - 1)^2}{2(\alpha^2 + 1)}} - B\right], \tag{A22}$$

where

$$B = \sqrt{\frac{1}{E_b K_f}}\,\frac{F^{\text{feed}}}{2\epsilon_b S}.$$

The lefthand side (Y) of Eq. A21 is plotted in Figure A1 vs. α for different B values. If (1)$\alpha \le 3$ and $B \ge 1$, or (2)

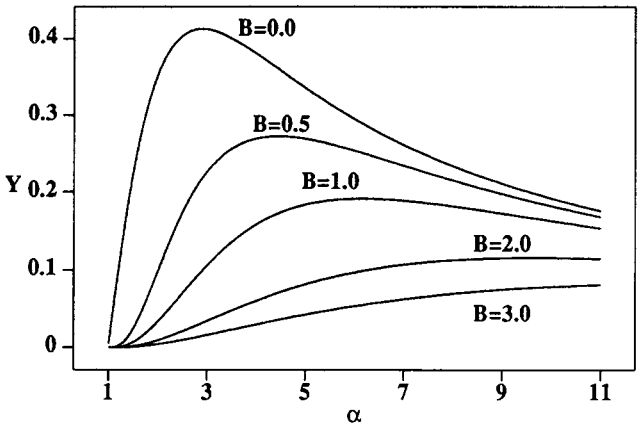

Figure A1. Plot of lefthand side of Eq. A21 vs. α at different B values.

$B \geq 2$ for all α, Y is less than 0.1 and Eq. A19 can be assumed. The B values can be small only if either E_b is large and/or K_f is large. When K_f is large ($K_f \geq 5$ in the example shown next) the equilibrium solutions (Eqs. 36 to 40) can be used and the assumption in Eq. A7 is not needed. Another point is that for systems with a small α, Y decreases with decreasing α. Therefore, Eq. A7 can be assumed for a large class of systems, especially for those with closely eluting solutes and large mass-transfer resistances. *Note that the preceding analysis is valid only for the standing waves.*

An example is shown for a system with the following parameters: $B^{\mathrm{I}} = 0.07635$, $B^{\mathrm{II}} = 0.07299$, $K_f^{\mathrm{I}} = K_f^{\mathrm{II}} = 5$, $E_b^{\mathrm{I}} = 1.2224$, $E_b^{\mathrm{II}} = 1.1171$ $\nu = 1.71233$, $\delta_1 = 0.56$, $\delta_2 = 0.69$, $u_0^{\mathrm{I}} = 3.1071$, $u_0^{\mathrm{II}} = 2.8420$, $P = 1.2222$. The eigenvalues from Eq. A13 for solute 2 (standing in zone I) are found to be $r_+ = 5.40279$ and $r_- = -0.03158$; for solute 1 (standing in zone II) $r_+ = 6.25711$ and $r_- = -0.03157$. From Eq. A17 $r_- = -0.03176$ for solute 2 in zone I and $r_- = -0.03173$ for solute 1 in zone II. Note that although $B^{\mathrm{I}} = 0.07635$ and $B^{\mathrm{II}} = 0.07299$, which are small values, the differences between the solutions from Eq. A13 and A15 are very small. Thus, because $\alpha = 1.231$ is small, the solution from Eq. 17 is still a good approximation of the solution of Eq. A11. These results are obtained with $Y^{\mathrm{I}} = 0.08856$. In general, when Y is less than 0.1 the solutions of Eq. A17 are close to those of Eq. A11.

Manuscript received Oct. 21, 1996, and revision received May 8, 1997.